

# **Characterization of Sewage Sludge Hydrochar for Use as a Heavy Metal Adsorbent**

by

Hunter Wieckowski

A Thesis

Submitted to the Faculty of the

WORCESTER POLYTECHNIC INSTITUTE

In partial fulfillment of the requirements for the

Degree of Master of Science

in

Chemical Engineering

---

August 2023

APPROVED:

---

Professor Michael Tim, Thesis Advisor

---

Professor Aaron Deskins, Committee Member

---

Professor Bruce Bursten, Committee Member

## **Abstract**

Alternative methods of managing sewage sludge have become a topic of increasing interest as traditional disposal methods are becoming more regulated and costly due to environmental concerns. One promising alternative treatment method is hydrothermal carbonization, a thermochemical process that can convert wet biomass to a higher energy-dense solid known as hydrochar. Hydrochar produced by SoMax Circular Solutions was characterized and the adsorption of Cu(II) ions was measured and compared to designer glucose hydrochar whose structure is more well-understood. Multiple analysis methods including FTIR, Raman spectroscopy XRD, and Boehm titration were employed. The high ash content of the hydrochar was found to influence the results making a direct comparison to other hydrochar difficult. The maximum adsorption capacity of the SoMax hydrochar was found to increase from 22.6 to 49.0 mg Cu(II) g<sup>-1</sup> following chemical treatment with Potassium Hydroxide. Chemical activation was found to change the best fit adsorption model from Langmuir to a non-interacting dual site Langmuir. Sewage sludge hydrochar was determined to be a potentially promising Cu(II) adsorbent as secondary treatment was not required for detectable adsorption.

## **Acknowledgements**

Foremost I would like to thank Professor Timko, my advisor, for the continual advice and guidance he provided during this project. I would also like to thank Professor Deskins and Bursten for serving as part of my thesis committee along with Timko. Assistant Research Professor Geoffrey Tompsett was incredibly helpful with running XRD and Raman spectroscopy as well as providing insight while analyzing FTIR data. XRF data was collected with help from Doug Leonardi. I would also like to thank the entirety of the hydrochar sub-group whose insight and previous work laid the groundwork for this project. A particular thanks to Achilles Gatsonis for producing the Copper Nitrate Solution used in all adsorption tests and Karen Agro for her assistance in developing the adsorption testing methods and help with fitting the isotherms. I would also like to thank SoMax Circular Solutions for providing the sewage sludge hydrochar used in all experiments and providing this opportunity. Finally, I would like to thank my family and friends for their continual support while working on this project.

Contents	
Abstract.....	2
Acknowledgements .....	3
Introduction.....	5
Background.....	7
Treatment and Disposal of Sewage Sludge.....	7
Hydrothermal Carbonization.....	10
Hydrochar Characterization Techniques.....	13
Hydrochar Structure .....	16
Hydrochar Properties .....	18
Hydrochar Modification .....	19
Hydrochar Uses .....	20
Hydrochar Adsorption of Copper.....	21
Hydrothermal Carbonization and Hydrochar in Industry .....	23
Previous Work on SoMax Hydrochar.....	24
Methodology.....	26
Hydrochar Production and Sourcing .....	26
KOH Activation .....	27
Ash Content.....	28
FTIR Spectroscopy.....	28
Boehm Titration .....	28
Raman Spectroscopy .....	29
X-Ray Fluorescence .....	29
X-Ray Diffraction.....	29
Copper Adsorption .....	30
Results & Discussion.....	32
Inorganic Analysis.....	32
Organic Analysis .....	34
Copper Adsorption .....	47
Conclusions & Recommendations .....	55
References.....	57
Appendix .....	68

## Introduction

The United States alone produces a nearly estimated 7.18 million tons of dry sewage each year as a byproduct of water treatment [1]. While the specific composition of the sludge varies depending on its source, sludge is typically comprised of organic materials derived from mostly organic wastes, as well as hazardous materials such as heavy metals from industrial runoff and harmful microorganisms [2]. Due to these harmful contaminants, it can be expensive to properly dispose of sewage sludge as it needs to be treated before disposal. Processing sewage sludge accounts for roughly half the entire operating costs at wastewater treatment plants even though it only composes a few percent of the total volume of mass treated at these facilities [3].

Converting sewage sludge to hydrochar via hydrothermal carbonization (HTC) is a promising alternative to traditional treatment methods such as incineration and landfilling. HTC can convert wet feedstock such as sewage sludge and convert it to a more energy-dense carbonaceous solid material [4]. The ability to process wet feedstock is advantageous as it removes the need for a drying step in the treatment process that is necessary for traditional methods and other thermochemical reactions such as pyrolysis. Hydrochar has many potential uses including its use as solid bio-coal for combustion, conversion into fertilizer, and as a sorbent for heavy metal and organic compounds [5].

Many HTC wastewater treatment sites exist globally already, these plants primarily use their hydrochar as fuel or fertilizer [6]. There is an interest in using sewage sludge-derived hydrochar as a sorbent that can be used to treat wastewater potentially for use onsite of these treatment plants. SoMax Circular Solutions is one of these treatment plants that has expressed interest in using their hydrochar as a higher-value product sorbent and has provided hydrochar they produced on an industrial scale for characterization and heavy metal adsorption testing.

Hydrochar and HTC as a field has been growing area of interest in the scientific community in recent years. Much of the published hydrochar characterization has been on design hydrochar produced from simpler homogenous feedstocks than sewage sludge such as glucose. These designer hydrochar have been shown to have low heavy metal adsorption capacities without additional treatment [7]. Chemical treatment with potassium hydroxide (KOH) has been shown to greatly increase the adsorption capacity of designer hydrochar as it deprotonates oxygenated surface groups allowing for easier cation exchange with heavy metals in aqueous solutions [8].

If potassium is present in sewage sludge in non-trace amounts and has been shown to also be present in its derived hydrochar, then sewage sludge hydrochar should have a higher Cu(II) adsorption capacity than designer hydrochar. The goal of this work was to characterize unmodified and KOH activated SoMax Sewage sludge hydrochar and to measure their Cu(II) adsorption capabilities to see how it compares to glucose derived hydrochar. This paper will also seek to explain how KOH activation modified the hydrochar and relate it to the differences observed in Cu(II) adsorption. Specific focus will be given to identifying what role oxygenated surface groups such as carboxylates and involatile compounds play in Cu(II) adsorption. Further this paper will aim to fit the Cu(II) adsorption isotherm to a model to gain a better understanding of how physically hydrochar acts as a Cu(II) sorbent.

# Background

## Treatment and Disposal of Sewage Sludge

Sewage sludge, also sometimes referred to as biosolids, are a solid byproduct produced from wastewater treatment processes. The specific composition of sewage sludge produced varies depending on the source of the municipal waste, for instance, sludge from China contains less organic material than that of sludge sourced in developed countries [9]. The organic materials in sewage sludge are derived from mostly organic wastes and microorganisms, but it also contains hazardous materials such as heavy metals from industrial runoff [2]. Due to the composition of sewage sludge, if untreated it cannot be disposed of safely. Contaminants in improperly disposed sewage sludge can find their way into the environment as harmful pollutants and exposure to humans can lead to health concerns [10]. Processing sewage sludge accounts for roughly half the entire operating costs at wastewater treatment plants even the dry solids only compose 1-2% of the total mass treated at these facilities [3], [11].

The treatment and allowed disposal methods of sewage sludge have become increasingly regulated in recent decades as countries such as the United States have passed laws such as the Clean Water Act of 1972 and its amendments [12]. Similarly, Council Directive 86/278/EEC of the European Union, also known as the Sewage Sludge Directive, was passed to ensure that sewage sludge used in agriculture does not impact the environment [13]. Regulations such as these have been passed to reduce pollution caused by sewage sludge and municipal waste and increase environmental safety. However, these regulations have contributed to the high cost related to treating sewage sludge as they set limits on acceptable pollutant levels in disposed sludge and prohibit low-cost environmentally unfriendly disposal methods such as ocean dumping [14].

The three most prevalent uses of sewage sludge in increasing order in the United States are incineration 14%, landfilling 42%, and land applications 43%, with the other 1% incorporating all other disposal methods [15]. To reach the point where sewage sludge can be disposed of by any of these methods it must first be treated. Sewage sludge undergoes thickening and dewatering processes to decrease the amount of liquid and increase the solid content of the sludge. Drying methods vary between countries and treatment sites and include mechanical methods such as centrifugation and belt filter presses [16] as well as evaporation-driven methods such as drying beds [17]. Regardless of the method, it is time and energy intensive to reduce the water content of sewage sludge as large volumes must be continuously processed. Following this sludge typically undergoes processes such as anaerobic digestion or treatment with lime to lower the organic content present in the sludge and to remove harmful pathogens [3]. Further treatment may also be applied to the sludge depending on the desired final disposal method or usage.

Landfill disposal is the most prevalent disposal method of those discussed here in less developed countries as well as in members of the EU-12 [18]. However, it has become increasingly unsustainable as land for dumping sites is finite and has become increasingly scarce in many countries. Landfilling is decreasing in popularity even in countries that have abundant land resources for dumping sites such as the United States. New regulations along with landfill taxes and the reluctance of landfill operators to accept sewage sludge to do construction difficulties have increased the cost of this disposal method [19].

Land amendment disposal methods differ from landfill methods as they aim to use sewage sludge as a resource. Treated sludge can be used for land reclamation, fertilizer for agricultural land, and a variety of less common uses in places such as golf courses or home gardens [15]. This is because sewage sludge has high concentrations of nitrogen (N) and

phosphorus (P) [20]. Use as an agricultural fertilizer has specifically been increasing in usage as an alternative to conventional disposal methods [21]. Heavy metals such as copper (Cu) and lead (Pb) are common in sewage sludge due to industrial wastewater and rainwater runoff, these contaminants restrict the usage of sewage sludge as a land amendment as these metals as toxic and accumulated in the soil reducing soil productivity and increasing pollution [22]. There is also the concern that these toxic metals could find their way into groundwater.

To reduce the toxicity of sewage sludge being used for land amendment, heavy metals within the sludge are either removed or immobilized. Immobilization occurs when the heavy metals are converted into more stable states that have reduced mobility and lower bioavailability [23]. Methods for heavy metal removal include leaching, bioleaching, ionic liquid extraction, and electrokinetic remediation. sludge [24], [25]. Often immobilization is preferred, as removal methods are costly, time intensive, and have a varying degree of homogeneity [25]. Composting is a common method used to immobilize heavy metals in sewage sludge [26]. The addition of basic compounds [27], aluminosilicate materials such as fly ash [28], zeolites [29], and phosphorus-bearing materials [30] have also all been shown to immobilize or pacify heavy metals found in sewage sludge.

Incineration of sewage sludge is a mature thermal treatment method used to dispose of sewage sludge. There are several specific methods of incineration used to dispose of sewage sludge, but it is of note incineration broadly does not refer to thermochemical treatment methods such as pyrolysis or the later discussed HTC. Incineration is often an alternative method of disposal when there is a lack of land resources [31]. While land amendment and landfill methods contribute to land or water pollution, incineration of sewage sludge contributes to air pollution. Sewage sludge being used as incineration fuel must be dried to a lower moisture content than

sludge disposed of in other methods or else it can lead to combustion issues in the furnace [9]. Dewatered sludge has a moisture content of 80% [32], [33] and must be further decreased to lower than 30% to be an effective fuel [34]. Lowering the moisture content is achieved by traditional thermal drying or by metabolic heat generated by aerobic microorganisms decomposing organic matter [35]. Further dewatering treatments contribute to the cost of incineration methods along with the filtration of pollutant emissions produced. Nitrogen [36] and sulfur oxides [37] are prevalent air pollutants produced from sludge incineration that are regulated by the Clean Air Act in the United States and other regulations that aim to achieve similar goals globally.

The disposal methods detailed in this section are not a comprehensive list of all sewage sludge management methods, but a brief overview of the most popular and mature methods used globally. Many innovative methods to deal with sewage sludge are being investigated including thermochemical technologies such as pyrolysis [31] and use as alternative additives in cement [3].

### **Hydrothermal Carbonization**

Hydrothermal carbonization (HTC) is an exothermic thermochemical conversion method that converts organic material, typically waste such as sewage sludge into usable high-carbon content products [4]. The main product of HTC is the solid phase known colloquially as hydrochar, however, other usable phases including syngas and crude bio-oil are also produced in smaller amounts which vary based on conversion conditions. The main advantage of the HTC process against other similar thermochemical conversion methods is the ability of HTC to convert high water-content biomasses [38]. Feedstock for similar thermochemical processes such as pyrolysis used to create biochar must be dried before treatment [39] which can be time and

energy intensive limiting the economic viability. Due to this HTC is considered advantageous for the treatment of several high-water content waste sources including the previously discussed sewage sludge, animal manures [40] food [41], agricultural, and forestry [42] wastes.

The feedstock for the HTC process is comprised of organic matter, typically waste and water. The feed in the presence of oxygen is then subjected to temperatures ranging between 180-250 °C for residence times varying between 1 and 72 hours [43]. During this period, the feed is under an autogenic pressure of 2-6 MPa [44]. The process produces a liquid slurry as well as small amounts of syngas. In laboratory settings, the gaseous phase of HTC is small and often not captured and instead lost to the environment. The slurry contains solid hydrochar which can be separated by filtration and an oil and aqueous phase which can be separated by a rotovap or other method.

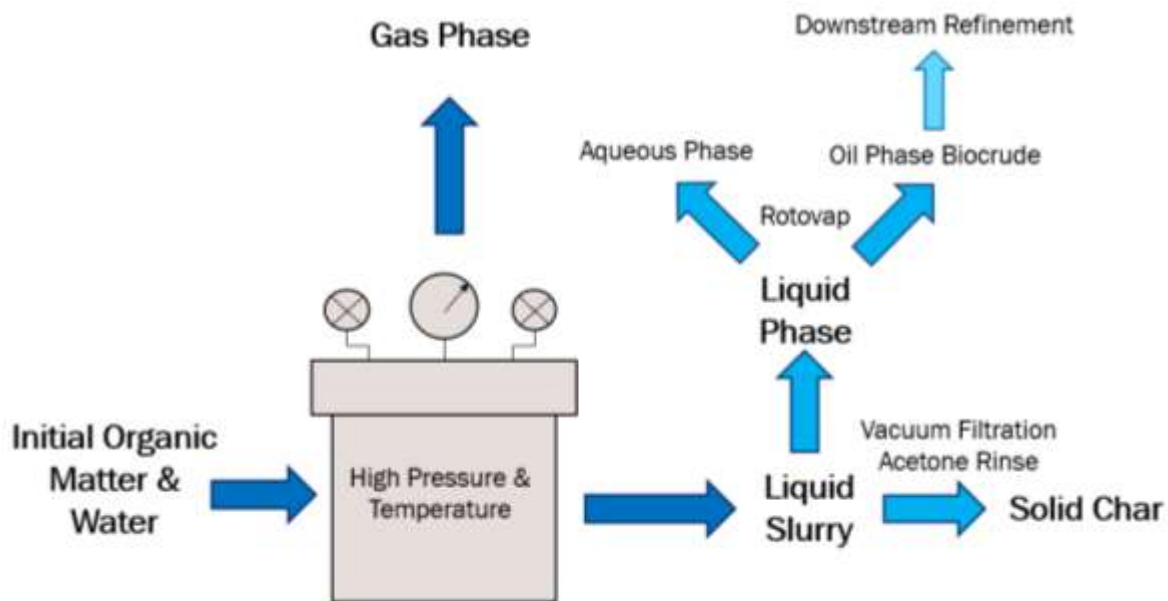


*Figure 1: Diagram of HTC Process from Feedstock to Separated Phases*

The heated aqueous conditions of the HTC cause the degradation of organic molecules, cellulose, hemicellulose, and lignin [45]. Biomass subjected to HTC is thought to be governed by

hydrolysis due to its lower activation energy. During hydrolysis, the bonds of the ester and ether bonds of the lignocellulosic biomass are broken [46]. Dehydration and decarboxylation are then thought to occur and to be responsible for reducing the H/C and O/C ratio of the hydrochar. Proteins when present in feedstocks are converted to smaller molecular weight peptides by hydrolysis reactions. The primary mechanisms of amino acid decomposition have been identified as deamination and decarboxylation [47]. Lipids in the form of fatty acids are also broken down by hydrolysis [48]. The reactive chemical fragments formed by the decomposition processes are subject to recombine by a series of condensation, polymerization, and aromatization reactions [43] resulting in the final hydrochar structure. These processes do not occur in a set order but instead in parallel making it difficult to understand specific chemistry. The mechanisms that govern HTC vary depending on the process parameters and feedstock used. Most of the work on understanding the kinetics and reaction pathways has been performed using hydrochar produced from model compounds such as glucose, and thus the reaction mechanisms of more complex biomass feedstock are less understood [48].

Operating conditions for HTC reactions are broad and there is not a universally accepted best method to produce hydrochar. Reactor conditions vary depending on the feed source with the goal of optimizing the hydrochar product ratio or a specific property of the solid hydrochar. There have been many papers published detailing and comparing HTC parameters used for different feedstocks. Literature on the topic suggests the most important parameters for the HTC process are the temperature of the reaction, followed by the time and water-to-organic material ratio of the feed [49]. The initial pH of the feed has also been shown to influence the conversion rates. The ratio of solid products produced has been shown to decrease with temperature, with temperatures above 250 °C favoring the production of liquid oil phases. It should be noted that

above 250 °C a different but related thermochemical process known as hydrothermal liquefaction (HTL) occurs. HTL is a more intense process than HTC and produces liquid biocrude as the main product. A third even more intense process occurs above temperatures above 374 °C. This process known as hydrothermal gasification (HTG) produces syngas as the main product. Both alternative processes produce some amount of solid hydrochar product, but HTC has the highest ratio of solid yield and is the focus of this paper. Residence time has been shown to have a similar but lesser effect on solid yield. It has been shown to be possible to get similar solid yields at different temperatures by varying the residence time, because of this sometimes a reaction severity parameter based on time and temperature is used to compare hydrochar produced by different methods [50].

The initial ratio of solid biomass to water also influences hydrochar yield. Experiments on a variety of feedstocks including miscanthus (a type of grass), glucose, and starch have shown that biomass-to-water ratios within the 1:5 to 1:8 range have the highest hydrochar yields [49]. In the same studies, higher ratios of biomass resulted in an increased gas phase and lower ratios of biomass increased liquid phases. Hydrothermal processes are carried out in reaction media with initial pH values below 7, as alkaline conditions can lead to substantially different products [43]. More acidic conditions,  $\text{pH} > 4.2$  have been shown to have a positive effect on the hydrochar yield [51], however, results have also indicated that the pH affecting additive itself may be more important than the initial pH [52].

### **Hydrochar Characterization Techniques**

This section will aim to discuss commonly used techniques to characterize hydrochar, specifically the methods used in this paper; Brunauer, Emmett, and Teller (BET) theory, Fourier transform infrared (FTIR) spectroscopy, Raman spectroscopy, Boehm titration, X-Ray

Fluorescence, (XRF), X-Ray Diffraction (XRD) and Inductively Coupled Plasma Mass Spectrometry (ICP-ms). It should be noted this is not an exhaustive list of methods used in literature to characterize hydrochar. Other methods such as Nuclear Magnetic Resonance (NMR), Near-Edge X-ray Absorption Fine Structure (NEXFAS), and X-ray photoelectron spectroscopy (XPS) are also commonly used to characterize hydrochar but are not necessary to understand the findings of this paper.

BET theory is a commonly used method to determine the surface area and porosity of samples [53]. In BET analysis a known amount of gas, usually N<sub>2</sub>, is released stepwise in a vacuum on a known mass of sample. If N<sub>2</sub> is used the solid surface is chilled with liquid N<sub>2</sub> to obtain detectable amounts of adsorption. During this time the gas molecules adsorb to the surface in a monolayer. The pressure of the cell is continuously and precisely monitored, and this is continued until a saturation pressure is reached indicating no more gas is being adsorbed to the surface of the sample. After the adsorption layers are formed the sample is removed from N<sub>2</sub> and heated allowing for the adsorbed nitrogen to be quantified. Using this data, a BET isotherm is constructed which plots relative pressure vs the volume of adsorbed gas. CO<sub>2</sub> is often used as a N<sub>2</sub> substitute for porous samples such as hydrochar due to concerns that N<sub>2</sub> at low temperatures is unable to penetrate complex porous microstructure [54].

FTIR, Raman spectroscopy, XRD, XRF, and Boehm titration are all used as methods to provide detail on the chemical composition of samples. FTIR is a nondestructive method to identify organic compounds within a sample. It works by subjecting samples to varying wavelengths of infrared radiation and recording the transmittance at these wavelengths. Infrared radiation induces vibrations either stretching or bending to the bonds of the atoms and different bonds and functional groups absorb different frequencies resulting in different identifiable

patterns in the recorded spectrum. These patterns can be used to identify specific bonds and functional groups present in the sample. FTIR is typically used as a qualitative tool.

Boehm titration is a quantitative method that can be used to determine the density of acid and base groups per mass sample. The technique works under the principle that weaker bases only oxidize stronger acidic sites on the hydrochar surface. Specifically, the weakest base Sodium Bicarbonate ( $\text{NaHCO}_3$ ) only reacts with the carboxylic acid sites which are the most acidic. Stronger bases such as Sodium Carbonate ( $\text{Na}_2\text{CO}_3$ ) react with carboxylic acid sites and less acidic lactonic groups. Finally, the strongest bases such as Potassium Hydroxide (KOH) react with all acid surface groups including phenolic groups. Through the difference in back titration using solutions of the bases listed, it is possible to determine the surface density of the acidic surface functional groups [55].

Raman spectroscopy works based on the principle of Raman scattering, which occurs when light interacts with a sample and the scattered photons have a change in energy. This happens in approximately 1 in 10 million photons [56]. In Raman spectroscopy light from a monochromatic laser usually in the visible near-infrared or near-UV range, is shown on a sample and the scattered photons are collected by a detector which can measure the intensity of the scattered light as a function of the light's wavelength [57]. Similarly, to FTIR it is possible to determine the molecular structure of the sample by interpreting and comparing the bands produced to those of known samples. Typically, Raman spectroscopy is a nondestructive characterization method. However, samples sensitive to heat such as hydrochar can be thermally modified by the applied laser at high energy intensities [58].

XRD is a technique used to identify crystalline structures present in samples [59]. X-ray radiation typically from a cathode ray tube is emitted onto a sample and as the rays pass through

the sample they are scattered. The pattern in which the rays are scattered is known as the diffraction pattern which is characterized by distinct peaks which correspond to the angles that constructive interference occurred when the X-rays were scattered. Peak position is related to the atom spacing of the crystalline structure by Bragg's [60]. Using Bragg's law and the measured scattering angles and intensities it is possible to determine atomic arrangement within a crystal structure, however, most crystalline structures have already been determined so peaks can be compared to that of known standards.

XRF is a common nondestructive technique used to determine the elemental composition of a sample. It works by emitting high-energy radiation onto a sample that excites the atoms of the sample which emit their inner orbital electrons [61]. When outer electron orbitals fill in the inner shell X-ray fluorescence radiation is emitted, which a spectrometer can measure. Each element fluoresces differently and by collecting the photon counts of the atoms that fluoresce it is possible to determine a quantitative elemental composition. Most XRF devices are not able to accurately detect light elements with atomic numbers  $<16$  [62].

ICP-ms is another analytical method used to determine the quantitative elemental composition of a sample. Unlike XRF, ICP-ms is a destructive technique and the samples must be liquid. Small amounts of the liquid sample are aerosolized using Argon (Ar) gas which is then atomized and ionized by Ar plasma [63]. The ions are refined by a series of lenses that guide the ion beams into a quadrupole mass analyzer after which point, they are separated by their mass/charge ratio allowing for the spectrometer to detect and report elemental composition [64].

## **Hydrochar Structure**

Currently, there are several proposed structural models for hydrochar derived from homogenous feedstocks such as cellulose and glucose using a variety of methods including

FTIR, NMR, NEXFAS, Raman spectroscopy, and XPS. While these proposed models differ, they all suggest the presence of an aromatized carbon backbone with oxygenate functional groups. The skeletal structure of hydrochar is comparable to that of naturally forming coal with an increased number of functional groups, specifically oxygen-containing ones [43]. Schmidt-Rohr from Brandeis University proposed a glucose hydrochar model based on experimental NMR data that featured a mixed backbone of furan and arene ring structures, with several carboxylic, lactonic, and phenolic functional groups present [65].

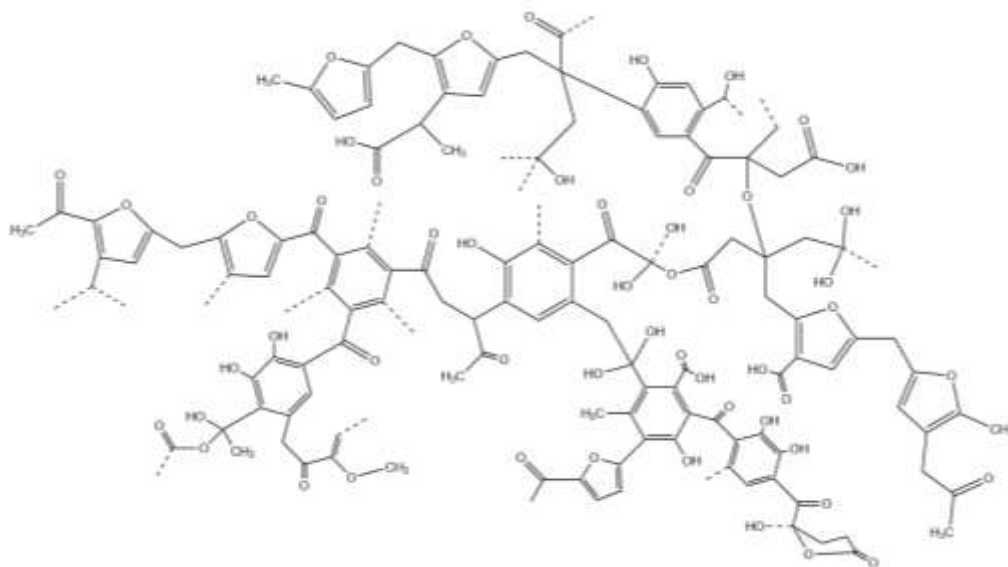


**Figure 2:** Proposed Glucose Hydrochar Structure Based on NMR data by Professor Schmidt-Rohr et al., Brandeis University, unpublished [65]

Previous groups such as Chuntanapum [65] have instead proposed arene-rich structures based on IR and Raman data. However, it has been shown that lasers used in Raman spectroscopy can induce thermal artifacts if used above power densities of  $5\mu\text{W}\ \mu\text{m}^{-2}$  [58]. Structures derived from Raman at lower power densities are more consistent with furanic NMR structures [58]. Similarly, the temperature of the HTC reaction has been shown to alter the arene

to furan ratios with arene increasing with temperature above 200°C [67], [68]. Other models such as that proposed by Sevilla and Feuertes [69] on cellulose hydrochar presented a structure composed of clusters of condensed benzene rings. Cellulose is a more thermally stable molecule than glucose and has not been shown to exhibit furan-rich structures like glucose char even when produced under the same process conditions [67].

To date, there are no available proposed detailed structures for sewage sludge hydrochar, although it would reason it would share some similarities with hydrochar produced from simpler feeds. This is backed up by experimental FTIR data from several groups that indicated the presence of similar oxygen functional groups and aromatic rings [70], [71]. The ash content of sewage sludge-based hydrochar has been shown to differ greatly from hydrochar produced from pure biomass due to the nature of sewage sludge. Elemental analysis has also shown the ash weight percent in sewage sludge hydrochar [71] to be greater than that of biomass hydrochar.

### **Hydrochar Properties**

As with yield, the physicochemical properties of hydrochar vary depending on feedstock and process parameters, most importantly process severity. In general, hydrochar has a poor surface area and pore volume when compared to other similar biomass-derived materials such as biochar from pyrolysis and activated carbon [72]. Typically, hydrochar surface area is <50 m<sup>2</sup>g<sup>-1</sup> [5], [69] [72], [73], [74], [75], although higher values are uncommonly reported in the literature. This is much lower than commercial activated carbons which can have surface areas in the 1000s m<sup>2</sup>g<sup>-1</sup> and biochar which commonly has surface areas >100s m<sup>2</sup>g<sup>-1</sup> [5], [76]. As HTC process severity increases the surface area of hydrochar has been found to increase.

Oxygenated functional groups are the main property of hydrochar that are the focus of this paper. FTIR analysis of hydrochar has routinely identified carboxyl, hydroxyl, carbonate, alkane,

aromatic, alcohol, ester, ether, and ketone groups to be present [76]. Hydrochar has a larger amount of oxygen functional groups than activated carbon [78] and naturally forming coal [43]. These functional groups have been found to play a key role in the sorption of heavy metals [8].

### **Hydrochar Modification**

Often hydrochar is further modified after being separated from the liquid slurry. This is to enhance the properties of the hydrochar to increase its performance in a desired area of application. For instance, for industrial adsorbent applications hydrochar may undergo secondary treatment to increase its surface area and porosity [7], [72] to enable a higher adsorption capacity. Secondary treatment methods include physical, thermal, and chemical processes. Physical methods activate hydrochar by subjecting it to heated CO<sub>2</sub> or steam streams. Thermal methods similarly heat dry hydrochar but in air or air and N<sub>2</sub>. Chemical methods modify hydrochar with the use of a chemical catalyst [79] in an aqueous solution. Chemical activation is achieved by submersing the hydrochar in an aqueous solution typically at normal temperatures, but it may also be carried out at elevated temperatures.

The most common chemical catalyst used in hydrochar activation is potassium hydroxide (KOH) [7], although additives such as zinc chloride (ZnCl<sub>2</sub>), phosphoric acid (H<sub>3</sub>PO<sub>4</sub>) [80], and iron chloride (FeCl<sub>3</sub>) [81] are also used. Chemically activated hydrochar has been shown to have a significantly increased surface area as well as increased adsorption capacities for organic molecules [82] and heavy metals [8]. KOH treatment has also been shown to generate additional oxygenated functional groups [83], [84].

The use of a chemical catalyst may require the hydrochar to undergo additional post-treatment such as washing which increases cost [80]. It also requires the safe disposal of the additives themselves to avoid contamination. Both air-activated and CO<sub>2</sub>-activated hydrochar

have been shown to have increased surface area comparable to that of chemically activated hydrochar [85]. Physical methods have also been shown to have a more well-developed microporous structure than unmodified hydrochar but decreased mesoporosity. They have also been shown to have a decreased amount of oxygen surface groups [86]. Thermal activation methods in air have been shown to have the opposite effect of increasing the amount of oxygenated functional groups while increasing mesoporosity [80].

### **Hydrochar Uses**

Hydrochar can be applied to a variety of applications depending on its specific physicochemical and morphological properties. Widely investigated areas of application include use as a soil amendment or fertilizer, use as a solid biofuel, and as an adsorbent for heavy metals and organic compounds [5]. Hydrochar is also being considered for use in electrochemical devices such as supercapacitors and batteries due to having lower surface area, polarity, porosity, aromatic structure, and general stability [5].

Soil amendment is a commonly suggested use for hydrochar, as depending on the feedstock the material is commonly rich in important elements that soils may be deficient in such as C, P, K, and N [87], [88]. Hydrochar regardless of feed source, untreated or in large amounts has been shown to have phytotoxic effects [89]. The phytotoxic effect of hydrochar has been attributed to organic compounds such as furans, polyaromatic hydrocarbons, and carboxylic acids [90]. Heavy metals are attributed to lower plant growth when they are present in hydrochar composition. Washing [91], aging [89] and aerobic treatment methods [92] have all been shown to reduce the phytotoxic effect of hydrochar and have a positive effect on plant growth. Washing methods have been shown to remove large amounts of phytotoxic compounds but do create another waste stream that must be dealt with. Other methods allow for the degradation of

phytotoxic compounds. Hydrochar as a compost additive has been shown to greatly improve plant growth more than compost alone [89]. To date, there are no commercially available hydrochar products marketed for soil amendment use [93]. Literature suggests more work on the topic, specifically the blending of hydrochar with other materials for soil amendment use [89], [93], [94], as well as the continuous long-term effects of hydrochar as a soil additive [91].

HTC converts low energy-density biomass into higher energy-dense hydrochar [95] that can be used as a potential alternative to traditional fossil fuels, specifically coal. The increased energy density is attributed to a decrease in cellulose and hemicellulose content during HTC and an increase in C/O ratios [5]. Studies using a variety of different organic waste feedstocks have shown that hydrochar can improve fuel performance and lower greenhouse gas emissions [96]. Hydrochar produced from food waste has also been shown to be a suitable substitute for conventional coal [97]. Alternatively, the gasification of hydrochar has been determined to be an effective method of producing hydrogen-rich syngas [98].

Adsorption is the process where one material in solution, the adsorbate transfers from a bulk solution to the surface of a second material the adsorbent. One of the more common uses of hydrochar is as an adsorbent for organic compounds such as dyes and pharmaceuticals as well as heavy metals including copper and lead [99]. Adsorption is a popular method for dealing with contaminants in water streams as it is associated with low cost to setup and maintenance [100]. Hydrochar from a variety of biomass sources has been shown to have heavy metal adsorption capacities comparable to commercially available activated carbon [101].

### **Hydrochar Adsorption of Copper**

Electrostatic interactions have been found to be the main driving force behind the adsorption of Cu to hydrochar. Cu(II) ions have a positive charge and due to the abundance of

oxygen functional groups the surface of hydrochar has a partial negative charge. Work by Delahaye and Hobson [8] indicated that carboxylate sites specifically have an important role in the Cu(II) sorption. Further Density Functional Theory (DFT) work by Gatsonis [101] expanded on this work suggesting hydroxyl groups specifically phenolic groups also play a key role in Cu(II) sorption.

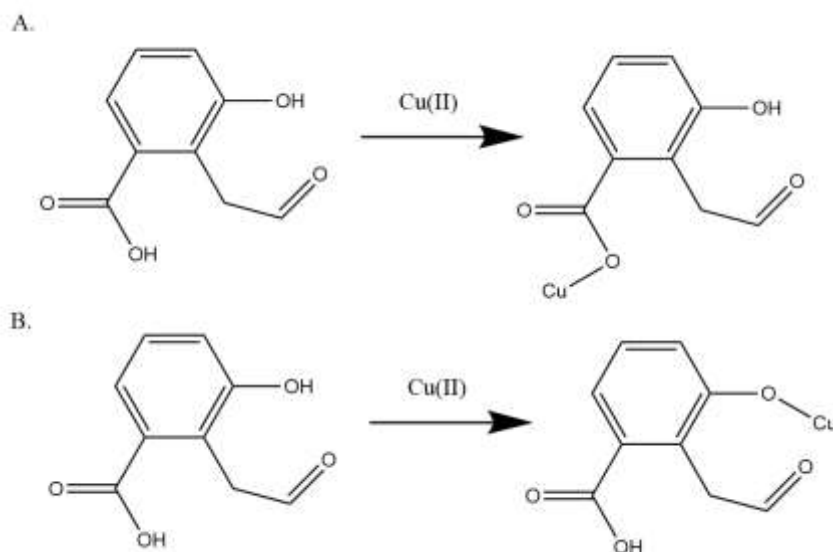


**Figure 3:** Potential Carboxylic (A), Phenolic (B) Copper Glucose Hydrochar Acid Group Binding Sites based on Unpublished Proposed Schmidt-Rohr Structure, Stoichiometry Based on DFT Calculations by Gatsonis

Unmodified hydrochar is typically not a good sorbent for heavy metals. Delahaye and Hobson [8] were not able to detect any Cu(II) adsorption when using unmodified glucose hydrochar. After alkali activation with either base, KOH or NaOH Delahaye and Hobson's hydrochar exhibited increased adsorption capacities, with KOH activated hydrochar having the higher of the two with a reported adsorption capacity of 40 mg Cu g<sup>-1</sup>. Alkali treatment deprotonates the hydrochar surface groups allowing for a higher level of coordination with

Cu(II) ions a thus a higher adsorption capacity [103]. Delahaye and Hobson's FTIR data showed a reduced intensity of the O-H stretch between 3200-3400 cm<sup>-1</sup> indicating partial deprotonation. This idea was further backed up by DFT simulations of cation binding that suggested the replacement of H<sup>+</sup> with Cu(II) was energetically unfavorable with the replacement of K<sup>+</sup> and Na<sup>+</sup> being favorable.

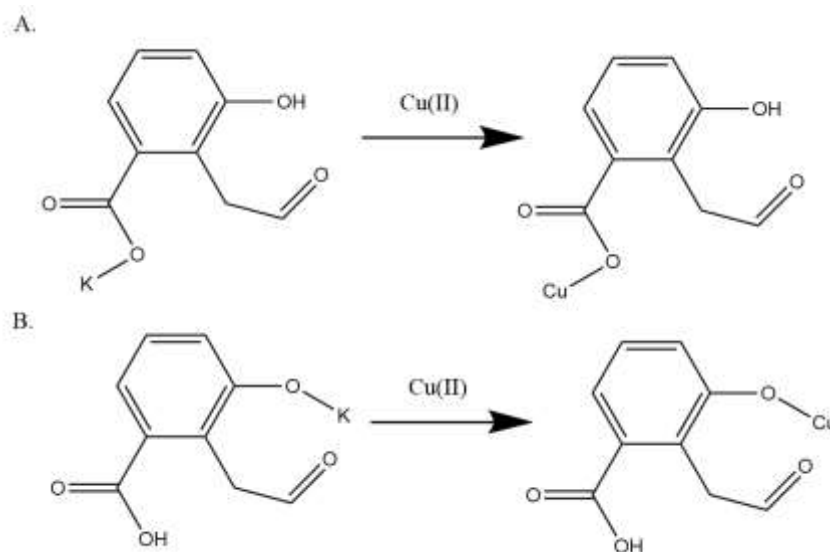


**Figure 4:** Potential Carboxylic (A), Phenolic (B) Copper KOH Activated Glucose Hydrochar Acid Group Binding Sites based on Unpublished Proposed Schmidt-Rohr Structure, Stoichiometry Based on DFT Calculations by Gatsonis

While the work by Delahaye and Hobson is based on glucose hydrochar it would reason that a similar mechanism occurs during sewage sludge hydrochar chemical activation if they are believed to have similar structures.

### Hydrothermal Carbonization and Hydrochar in Industry

More than 200 companies [7] and organizations engage in HTC processes worldwide, and a patent search for hydrothermal carbonization reveals more than 1,400 results. Industrial-

scale HTC plants have been around for more than a decade, with several European groups launching plants in 2010. The first recorded HTC plant on the industrial level was designed and operated by the Swiss company AVA-CO2 in Germany. Other companies HTCycleAG [104] and Ingelia [105] also launched their industrial plants in the same year in Germany and Spain respectively. Since then, these companies and other European companies including C-Green, Suncoal, Antaco, and Biokol have patented unique HTC processes [46]. Currently, HTC plants have been constructed in European countries including The United Kingdom, Italy, and Finland. Outside of Europe industrial scale HTC facilities are less common. The first HTC wastewater treatment site in North America was designed by SoMax Circular Solutions and began operating out of Phoenixville Pennsylvania in 2021 [106]. In 2022 an HTC wastewater processing plant in Mexico City began operations. China has been using HTC methods to treat sludge since 2016 [107].

Early HTC plants were able to process less than 10,000 tons of waste per year but locations such as the one in Mexico City can handle over 20,000 tons of waste annually. The largest HTC facilities currently planned for construction have the capacity to process upwards of 80,000 tons of waste annually [7]. The primary use for hydrochar produced at industrial plants is as bio-coal for energy production and fertilizer for land amendment applications. The biggest issue these facilities currently face is the handling and disposal of process water and other byproducts of the HTC process.

### **Previous Work on SoMax Hydrochar**

To date, SoMax has published 16 studies on hydrochar including work by Urbaniak [75] to test sewage sludge char as an adsorbent for methyl blue dye. Urbaniak produced their hydrochar for their work using the same source of sewage sludge as the hydrochar used in this

study. The process parameters for their sludge production were 20% solid content in a 200 mL stainless steel chamber at 200°C for 2 hours. This was based on work by SoMax's Chief Sustainability Officer Jeremy Taylor to be representative of the commercial scale [106].

Urbaniak tested the adsorption capacity of methyl blue for several different thermally and chemically modified versions of their hydrochar and compared it to commercially available activated carbon. Their unmodified hydrochar was able to adsorb 175mg/g of methyl blue, half commercially available activated carbon. Thermally activated hydrochar at 800°C performed much worse than unmodified hydrochar while chemically activated hydrochar at 3:1 KOH ratio was able to adsorb near the same amount as activated carbon. The decrease in the thermally modified hydrochar performance was theorized to be due to the expansion of pore sizes leading to a decreased surface area and change in surface group functionality [75].

Using BET surface area theory, the unmodified hydrochar was found to have a surface area of 15.77 m<sup>2</sup> /g while the highest performing hydrochar was found to have a surface area of 134.07 m<sup>2</sup> /g which while near an order of magnitude larger was still 10 times smaller than the surface area of the commercially activated carbon 1367.11 m<sup>2</sup> /g. Urbaniak confirmed that the adsorption was due to both surface area and the surface functional groups due to the much lower surface area of the hydrochar compared to the activated carbon. An inorganic analysis was performed on the three previously mentioned samples three samples using ICP-ms. The analysis revealed that the activated hydrochar sample had a much greater amount of K than the unmodified hydrochar indicating that K from activation stays in the sample and is not completely removed after washing [75].

## **Methodology**

### **Hydrochar Production and Sourcing**

Two types of hydrochar were used in this study, the main char of interest was produced by SoMax circular solutions from sewage sludge in the Phoenixville suburb of Philadelphia [106]. This char was produced in large quantities on the commercial scale, and all experiments using sewage sludge char were performed using samples from one batch of char. The other type of hydrochar used in this study was produced from glucose. The structure of glucose hydrochar is thought to be much simpler and more understood than chars produced from more complex feedstocks thus it was used as a standard in several instances to compare to the SoMax sewage sludge hydrochar.

The glucose hydrochar used in this study was made in several much smaller batches all using the following method. 28.152 g of D-glucose was added to a beaker containing 50 mL of deionized (DI) water while continually stirring. After the D-glucose was added another 50 mL of DI water was added and the solution was stirred until the D-glucose was fully dissolved. The solution was then poured into a PTFE-lined, stainless-steel autoclave which was then tightened and put into a room-temperature oven. The oven was then turned on to 180 °C and held at this temperature for 8 hours. After this the autoclave was allowed to remain sealed in the oven for a further 12 hours to allow cooling. After the cooling period ended the solution was removed from the autoclave and the resulting slurry was separated using vacuum filtration. The solid products were washed with a solution composed of 100 mL of ethanol and 100 mL of DI water for 20 minutes, before being vacuum filtered again. This washing step was repeated twice. The washed solid was then placed on a crucible and placed in an oven at 65 °C and allowed to dry for 24

hours. After this, the hydrochar was stored in an airtight vile for use. This method was adapted from previous work by Delahaye, Hobson, and Moran. [8], [65].

### **KOH Activation**

Hydrochar is commonly further modified after the initial HTC process to further tune desirable properties such as surface area and surface functional groups. There are many ways to modify or activate hydrochar both thermally and chemically, but activated hydrochar will exclusively refer to hydrochar that has been modified chemically by a KOH solution when discussing the work of this paper. The same procedure detailed below was used to chemically modify both the SoMax sewage sludge and glucose hydrochar and was adapted from Delahaye, Hobson [8].

56.12 g of KOH pellets were mixed in a beaker containing 400 mL of water. Once the KOH was added an additional 100 mL of DI water was added and the mixture was stirred until all the KOH was dissolved. 2.22 g of hydrochar was then weighed out and added to the mixture and stirred for an hour. Care was taken to ensure the hydrochar was fully mixed into the solution and did not remain mostly at the top. After one hour the solution was vacuum filtered and the solid material was placed into a separate beaker containing 50 mL of water and mixed for an additional 30 minutes. This second solution was then pH neutralized by the dropwise addition of 1 N hydrochloric acid (HCl) until the pH was in the range of 5-7. The solution was mixed for another 30 minutes to verify the pH was stable and in the desired range and additional HCl was added if needed. The neutralized solution was then vacuumed filtered and washed with 50 mL of DI water while on the filter. The wash step was repeated two more times after which the solid material was transferred to a crucible and placed in an oven at 100 °C for 24 hours to dry. After this, the hydrochar was stored in an airtight vile for use.

## **Ash Content**

To determine the ash weight percent of the hydrochar, samples of known weight were placed in a muffle furnace at 550 °C for 3 hours. After this period, sufficient time to cool samples was re-weighed to determine the mass loss attributed to volatile compounds.

## **FTIR Spectroscopy**

FTIR spectroscopy was performed on samples of both unmodified and KOH-activated sewage sludge hydrochar to gain a qualitative understanding of the functional groups present. Samples were run using a PerkinElmer Spectrum machine and a background scan was run to reduce signal contribution from the environment.

## **Boehm Titration**

Boehm titration was performed on unmodified and modified samples of the sewage sludge hydrochar as a method to determine the density of different oxygen-containing functional groups [108]. 20 mL solutions of 0.1 N HCl, 0.1 M NaHCO<sub>3</sub>, 0.1 M Na<sub>2</sub>CO<sub>3</sub>, and 0.1 M KOH were put into separate 50 mL tubes. 0.2 g of the hydrochar was then placed into each tube and mixed thoroughly for 48 hours. After the allotted mixing time ended the solutions were vacuum filtered. 5 mL of each of the 3 basic solutions were then taken and 5 mL of DI water and 5 mL of 0.1 N HCl were added. Similarly, 5 mL of the HCl solution from the shaker was separated. The solutions were then degassed for 1 hour using nitrogen to remove any carbon dioxide (CO<sub>2</sub>) that had diffused into the solutions. CO<sub>2</sub> can form additional base species that can change the results of the titration [108]. Each solution was then titrated with 0.1 M of Sodium Hydroxide (NaOH) until a pH of 7 was reached. Equation [1] was used for the basic solutions to determine the density of the acid sites and equation [2] was used for the HCl solution to determine the density of the base sites [65].

### *Acid Site Density*

$$= \left( \frac{n_{HCl}}{n_{Base}} [Base]V_{Base} - ([HCl]V_{HCl} - [NaOH]V_{NaOH}) \frac{V_{Base}}{V_{sample}} \right) \div m_{Hydrochar}$$

***Equation 1: Acid Site Density of Hydrochar determined from Boehm Titration***

$$Base\ Site\ Density = ([HCl]V_{HCl} - [NaOH]V_{NaOH}) \frac{V_{HCl}}{V_{Sample}} \div m_{Hydrochar}$$

***Equation 2: Base Site Density of Hydrochar determined from Boehm Titration***

### **Raman Spectroscopy**

Raman spectroscopy was performed using a Horiba Xplora device. Care was taken to ensure samples were analyzed using power densities less than 5 GW m<sup>-2</sup>, as it has been shown in the literature that Raman spectroscopy performed at power densities higher than 5 GW m<sup>-2</sup> can thermally induce a transition in the chemical structure of the hydrochar [58]. To achieve this a wavelength of 532 nm was used with a 1200 grating at 1% power for 5 intervals of 20 seconds.

### **X-Ray Fluorescence**

Unmodified and KOH-activated glucose and sewage sludge hydrochar were run using an ARTAX XRF spectrometer to determine the elemental composition of the hydrochar samples with a specific interest in Si, Fe, and K contents. To correct the error measured by the device, standard samples of Iron(III) Oxide (Fe<sub>2</sub>O<sub>3</sub>), Silica (SiO<sub>2</sub>), Carbon black, and a known mixture of the three were prepared.

### **X-Ray Diffraction**

XRD analysis was performed on samples of unmodified sewage sludge hydrochar to help determine the chemical composition and crystallographic structure. A Rigaku XRD machine was

used to perform the analysis. The analysis was performed using the following parameters: 25 mA, 37.5 kV, a degree step of 0.05, and a 1-second dwell time.

### **Copper Adsorption**

Single point Cu(II) adsorption was performed with the intent to produce isotherms for the unmodified and modified sewage sludge hydrochar. A buffer solution of pH 5 was made using sodium acetate ( $C_2H_3NaO_2$ ) and acetic acid ( $CH_3COOH$ ). It has been shown in the literature that hydrochar has the highest adsorption capacity at pH 5 [9], [109]. The buffer solution was then combined with 0.05 M Copper Nitrate ( $Cu(NO_3)_2$ ) to make a 10 mL solution of the desired Cu concentration for each trial run. Next 0.2 g of hydrochar was suspended in the 10 mL Cu solution and placed on a shaker and mixed for a period of 24 hours to allow for maximum adsorption.

After the mixing period, the solid char was removed from the solution via vacuum filtration. Each liquid solution was run through the vacuum filter twice. Small amounts of the residual solid hydrochar were kept in case further analysis was deemed necessary. After vacuum filtration, the liquid samples were further filtered through a pipette filter to remove any small solid char residuals that made it through vacuum filtration. After the second round of filtration, the samples were then further diluted with DI water to 50 with a concentration of 10-200 ppb Cu so the samples would be in a concentration range the ICP-ms spectrometer could read. The samples were also acidified with 0.5 mL of Nitric Acid ( $HNO_3$ ) before being run for the same reason. This method was adapted from Delahaye and Hobson [8].

Before testing samples of each batch of Cu solutions, the ICP-ms machine was optimized and baselined with stock solutions of 10, 20, 50, 100, and 200 ppb Cu. The machine ran each sample in triplicates and returned the average concentration value which was used to determine

the equilibrium concentration and then the adsorption capacity of the Cu solutions after the mixing period. The adsorption capacity was calculated using equation 3 [66].

$$\text{Adsorption Capacity} \left( \frac{\text{mg}}{\text{g}} \right) = \frac{\text{Initial Mass of Cu} - \text{Final Mass of Cu}}{\text{Mass of Sorbant}} * 1000$$

***Equation 3: Copper Adsorption Capacity of Hydrochar***

Several samples were prepared throughout the testing process without the addition of any hydrochar. These samples were used to determine the accuracy of the calculated equilibrium concentration.

## Results & Discussion

### Inorganic Analysis

Incineration revealed the ash content of the unmodified hydrochar to be 56.3%, decreasing to 41.6% after activation a decrease of 14.7%. Lower ash content post-KOH treatment is consistent with findings in the literature, attributed to an enhanced pore structure increasing the amount of fixed carbon [110]. It is also possible the washing steps during the activation process physically removed some non-volatile compounds. Washing with other solvents including HCl and acetone has been shown to be an effective method of decreasing ash content [111]. After removal from the muffle furnace, the coloring of the hydrochar changed from a dark brown to an orange-red tint. This coloring, present in both KOH and unmodified samples could suggest the presence of Iron Oxide ( $\text{Fe}_2\text{O}_3$ ).



*Figure 5: Hydrochar Left to Right; Unmodified, Unmodified Ash, KOH Activated, KOH Activated Ash*

X-ray diffraction was used to gain an initial qualitative understanding of the ash composition in the SOMAX hydrochar. The XRD pattern shown in Figure 4 shows the presence of crystalline compounds, iron(II, III) oxide ( $\text{Fe}_3\text{O}_4$ ), and quartz. Bands at 30, 36, 43, 54, 56,

and  $62^\circ$  indicate the presence of  $\text{Fe}_3\text{O}_4$ , and the band at  $26^\circ$  indicates silica in its crystalline form quartz. The broad peak between  $5\text{-}25^\circ$  is representative of the amorphous hydrochar. Interestingly the form of iron oxide detected was  $\text{Fe}_3\text{O}_4$ , not  $\text{Fe}_2\text{O}_3$  despite the orange-red tint of the hydrochar ash. It is likely that during incineration  $\text{Fe}_3\text{O}_4$  was converted to  $\text{Fe}_2\text{O}_3$  and was not originally present in the ash, as this would explain the color change. This reaction has been shown to occur at temperatures above  $500^\circ\text{C}$  in air [112].

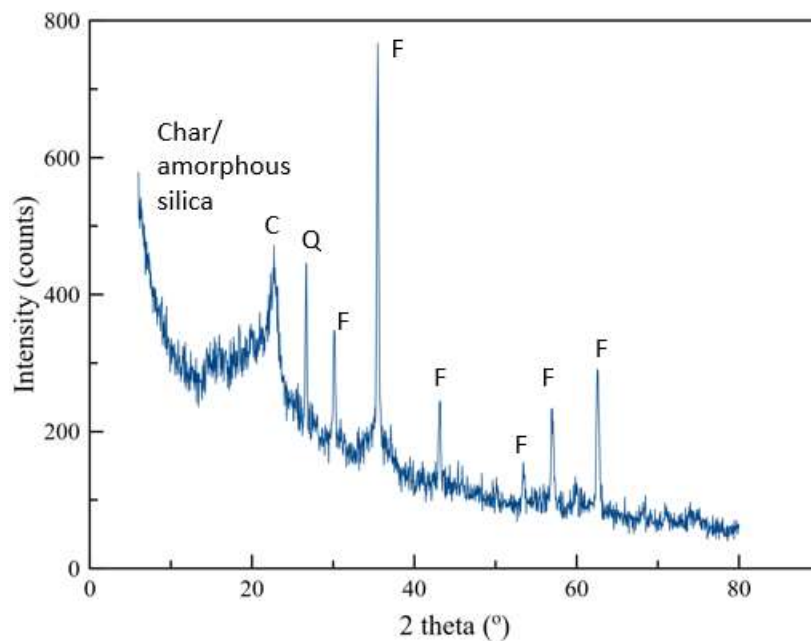


**Figure 6:** XRD Analysis of Unmodified SoMax Sewage Sludge Hydrochar. Labeled Peaks  $F$   $\text{Fe}_3\text{O}_4$ ,  $Q$  Crystalline Silica Quartz,  $C$  char

While it is difficult to discern specific features in the region between  $10\text{-}25^\circ$ , the sharp feature centered on  $22^\circ$  can be attributed to cellulose, indicating that the HTC process used by SoMax did not fully deconstruct the lignocellulosic biomass structure. If the process parameters used by Urbaniak are believed to be consistent with those used to produce the hydrochar given by SoMax

this would be consistent with findings from Sevilla and Fuertes that indicated temperatures >220 °C [69] are required for HTC to deconstruct cellulose.

Other unidentifiable peaks may be present in the XRD pattern that indicate the presence of other minerals in the ash content of the Hydrochar in trace amounts. Noticeably absent is the presence of pyrite (FeS<sub>2</sub>) which was detected by Luo and Huang in XRD samples of sewage sludge-derived hydrochar [113]. Due to the varying nature of sludge composition, FeS<sub>2</sub> may be present in a higher concentration in the sewage sludge used by Luo and Huang. Work by Xiao and Ding [114] on the composition of Fe species in sludge hydrochar found iron(III) Oxide (FeOOH) to be the most common form of Fe in their hydrochar and Fe in combination with elements P or S was not detected. FeOOH, Fe<sub>2</sub>O<sub>3</sub>, and other forms of Fe may be present in the sample, however, they could be below the detection limit of XRD.

XRF was able to detect Fe and Si in the SoMax sewage sludge samples which agrees with the results from XRD. Based on the results of the Silica and Fe<sub>2</sub>O<sub>3</sub> standard the relative ratio of the two compounds in the SoMax hydrochar was estimated to be 1:1. XRF was unable to detect the presence of K in any of the hydrochar samples which indicates it must be present in abundance to be detected. Fe and Si were the only elements detected in the SoMax hydrochar with other bands attributed to noise. The two glucose hydrochar samples had very low absolute band intensities compared to the standards and sewage sludge hydrochar indicating no heavy atoms presence in abundance.

### **Organic Analysis**

FTIR spectra of unmodified and KOH-activated SoMax sewage sludge hydrochar are shown in Figure 7. The spectra were normalized by intensity to the (CH<sub>n</sub>) band centered near 2800 cm<sup>-1</sup>. This normalization was chosen with the assumption that the KOH treatment would

not be sufficient to break or form covalent C-H bonds in the structure, but rather deprotonate functional groups [115]. In general, the band positions observed are in good agreement with previously reported FTIR spectra of sewage sludge hydrochar [116], [117], [118].

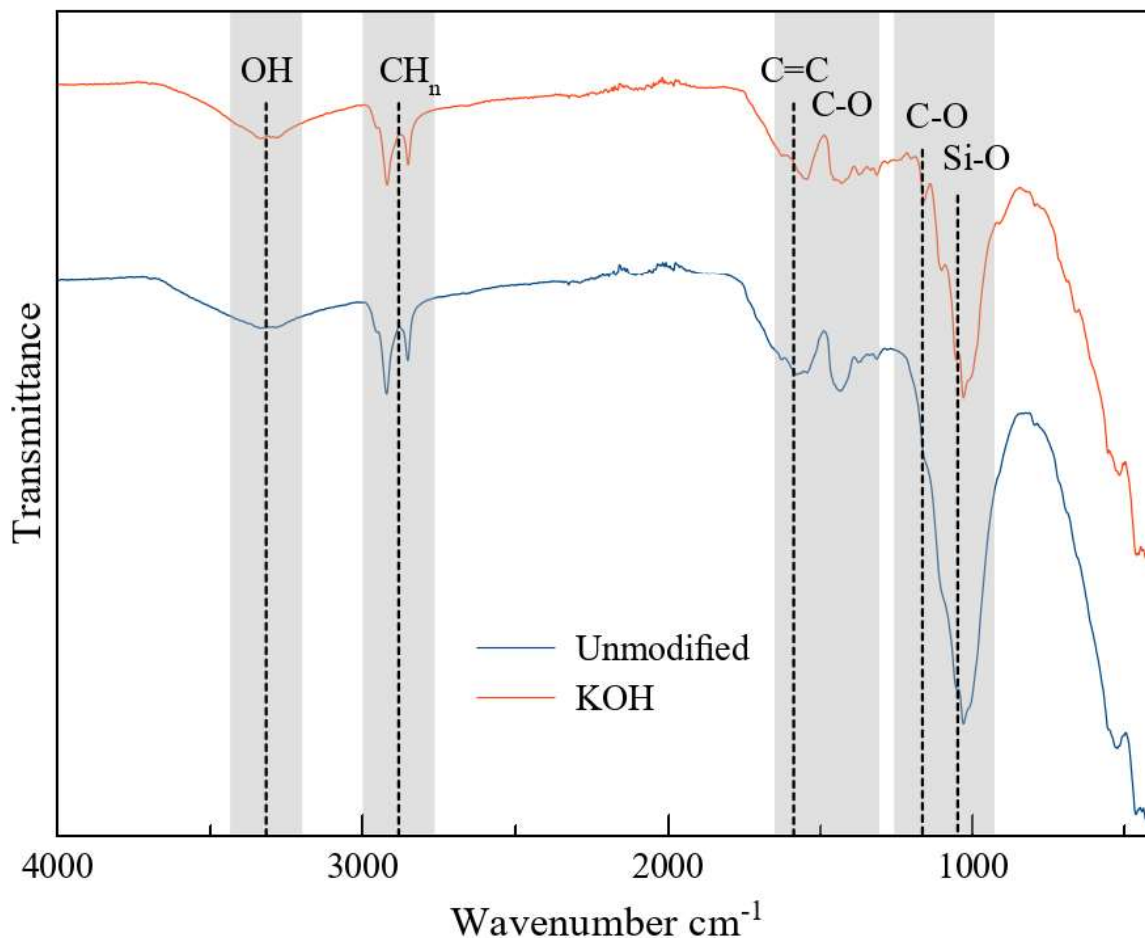


**Figure 7:** Complete FTIR Spectra of Unmodified and KOH activated SoMax Sewage Sludge Hydrochar

The two spectra were further subdivided into three segments to allow for better direct comparison and identification of functional groups, omitting areas not of interest. These segments can be seen in Figures 8, 9, and 10. Table 1 contains a list of the full band assignments.

*Table 1: FTIR Band Assignment*

<b>Band cm<sup>-1</sup></b>	<b>Assignment</b>	<b>Band cm<sup>-1</sup></b>	<b>Assignment</b>
3600-3000	O-H Stretching, hydroxyl, Carboxylic Acid [119]	1160	C-O-C Glycosidic Bonds [120]
2980-2875	C-H Asymmetric Methyl Group [116]	1310	O-H Phenol [117]
1627	C=O Amides [120]	1055	C-O Cellulose [118]
1650-1500	C=C Aromatic Rings [117]	1100-1030	Si-O Quartz [118]
1460-1430	C=C Furanic Ring [65]	912	Clay/Kaolinite [118]
1355	CH <sub>2</sub> Bending [118]	798	C-H out of Plane Bending [69]
1327-1123	C-O Stretching, hydroxyl, ester, ether [118]	560-500	M-O Metal Oxygen Stretching [120]

The broad band between 3600-3000 cm<sup>-1</sup> was widely attributed to O-H stretching from hydroxyl and carboxylic acid groups. This region was noticeably more pronounced in the KOH spectra indicating that alkali treatment established additional O-H bonds. This is consistent with claims in the literature that KOH activation increased the number of oxygen functional groups [84], [117] but disagrees with findings by Delahaye and Hobson who saw a decrease in O-H stretch intensity attributing the formation of K-O bonds [8]. This suggests that alkali activation established more oxygenated surface sites than O-H to O-K substitutions. It is also possible there are N-H stretches within this region from the presence of amines as sewage sludge is commonly high in N content [21]. This is further supported by the presence of a C=O amide bond at 1627 cm<sup>-1</sup> associated with proteins and lipids [117], [120]. However, no published papers on sewage

sludge hydrochar have given an amine assignment. Two distinct bands located at 2924, 2950, and 2853  $\text{cm}^{-1}$  were attributed to C-H stretching [116].

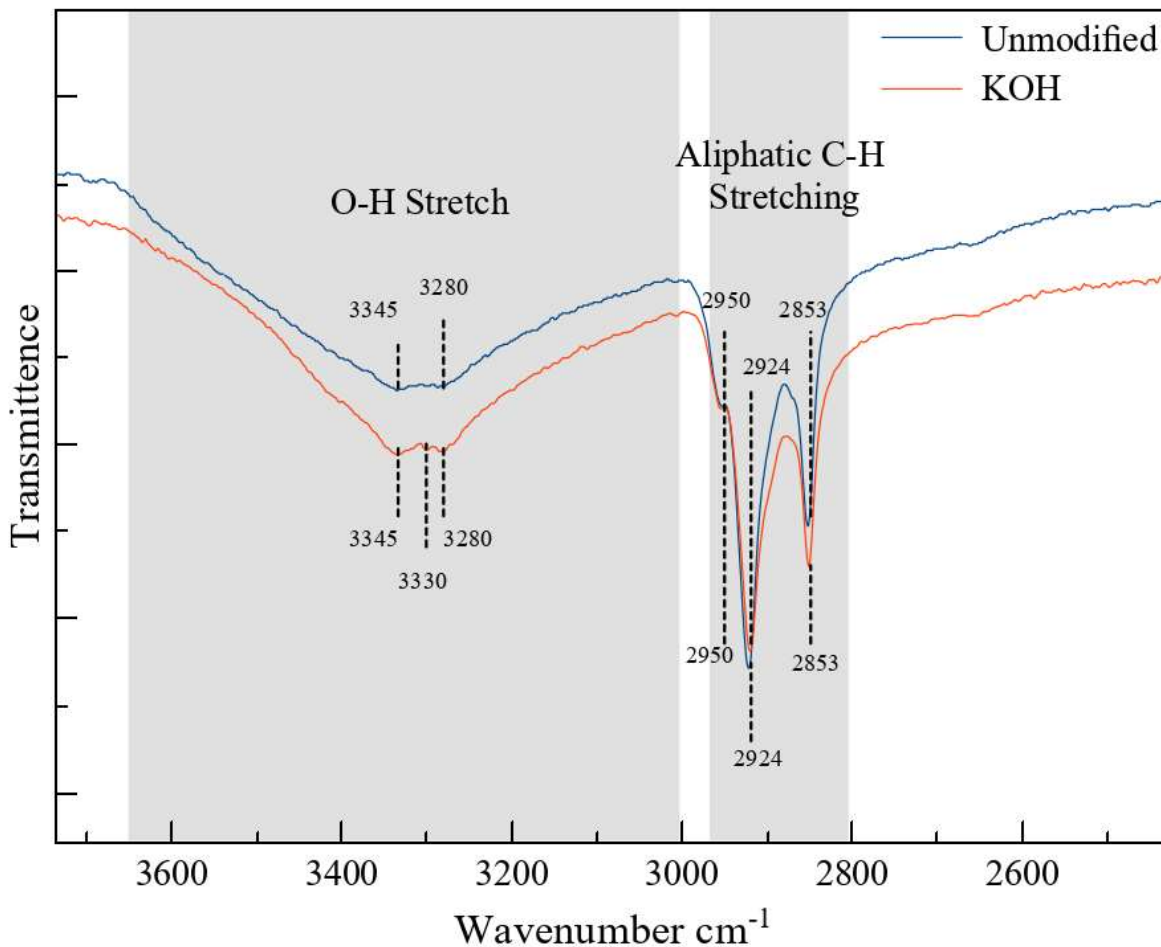


**Figure 8:** FTIR Spectra of Unmodified and KOH activated SoMax Sewage Sludge Hydrochar  
3900-2500  $\text{cm}^{-1}$

The band between 1650-1500  $\text{cm}^{-1}$  indicates the presence of aromatic structures and the band between 1460-1430 suggests the presence of furan rings. There may be furan/arene overlap in the 1650-1500  $\text{cm}^{-1}$  region [65]. This band is consistent with bands of glucose hydrochar indicating similarities in the two structures [8]. The region between 1327-1123  $\text{cm}^{-1}$  contains several bands corresponding to the C-O bonds of hydroxyl, ester, and ether groups [118]. This

region is more pronounced in the activated hydrochar. Of specific note is the band centered at 1310  $\text{cm}^{-1}$  which indicates the presence of phenol groups. Notably absent in either spectrum is a strong sharp band near 1700  $\text{cm}^{-1}$  representative of carboxylic acid, suggesting its absence in the hydrochar. Carbonyl C=O groups have been inconsistently reported in sewage sludge hydrochar FTIR spectra [136] [137]. The characteristic bands Alkali carboxylates have been shown appear near 1550 and 1430  $\text{cm}^{-1}$  for symmetric and asymmetric COO<sup>-</sup> stretching. It is possible these bands may be present and overlap with aromatic and furan bands [138] [139].

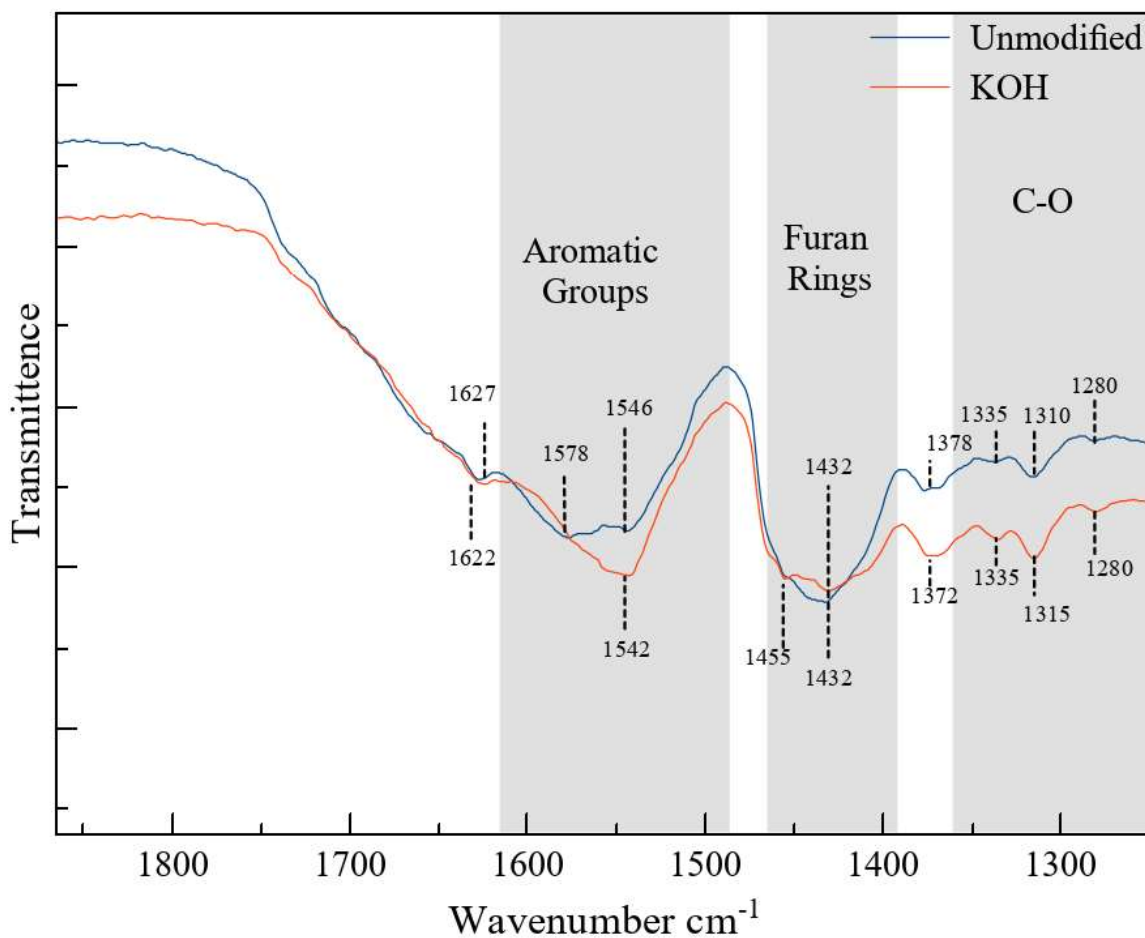


**Figure 9:** FTIR Spectra of Unmodified and KOH activated SoMax Sewage Sludge Hydrochar  
1950-1250  $\text{cm}^{-1}$

Bands at 1160 [120] and 1055  $\text{cm}^{-1}$  [118] indicate the presence of cellulose from C-O-C and C-O bonds respectively, this is consistent with results from XRD that indicated cellulose was not fully deconstructed in the HTC reaction. The large band 1100-1030 indicates the presence of Si-O bonds from quartz in the ash content of the hydrochar. This band is much less intense in the activated spectra due to a decreased ash content in the KOH hydrochar. Due to the prominence of the Si-O band, it is likely that several other bands in the vicinity that are not seen in the unmodified hydrochar; 1202, 1160, 1105  $\text{cm}^{-1}$  are being obscured and the representative groups are present in the compound.

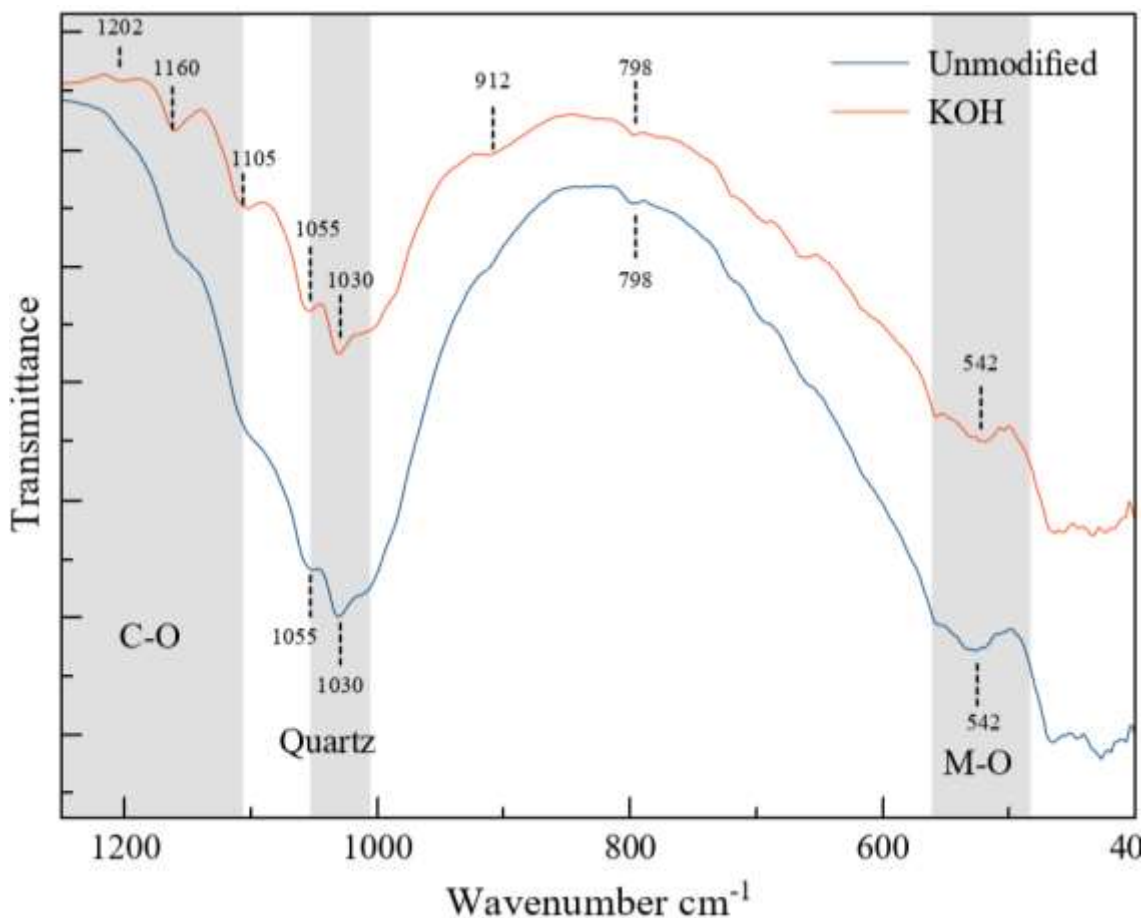


**Figure 10:** FTIR Spectra of Unmodified and KOH activated SoMax Sewage Sludge Hydrochar  
1250-400  $\text{cm}^{-1}$

The band at 798  $\text{cm}^{-1}$  is attributed to C-H out-of-plane bending [69]. The band at 912  $\text{cm}^{-1}$  is attributed to clay from soil in sewage sludge however other papers have attributed it to kaolinite ( $\text{Al}_2\text{Si}_2\text{O}_5$ ) [118] a common additive in the pulping industry. The 560-500  $\text{cm}^{-1}$  region indicates the presence of metal oxides such as iron and aluminum [120]. The presence of a metal oxide band is consistent with XRD and XRF which indicated  $\text{Fe}_3\text{O}_4$  in the ash composition.

Boehm Titration results can be seen in Figure 11. The total acid site density was shown to have slightly increased after activation. Phenolic and lactonic sites were shown to have increased while carboxylic sites decreased. Notably Boehm titration indicated the presence of carboxylic acid which is inconsistent with FTIR results. The acid site distribution in the unmodified hydrochar was nearly uniform while the activated hydrochar had a higher density of weaker acid sites. The results from Boehm titration support the notion that KOH activation increased the total amount of oxygen functional groups on the surface of the hydrochar. Results from Boehm titration would suggest that the increase in the O-H band intensity detected by FTIR is due to specifically an increase in hydroxyl groups not carboxylic acid. The decrease in carboxylic acid is potentially due to the deprotonation of carboxyl groups to carboxylate as Delahaye and Hobson suggested [8], which would indicate carboxyl sites are preferred for deprotonation over other acid sites.

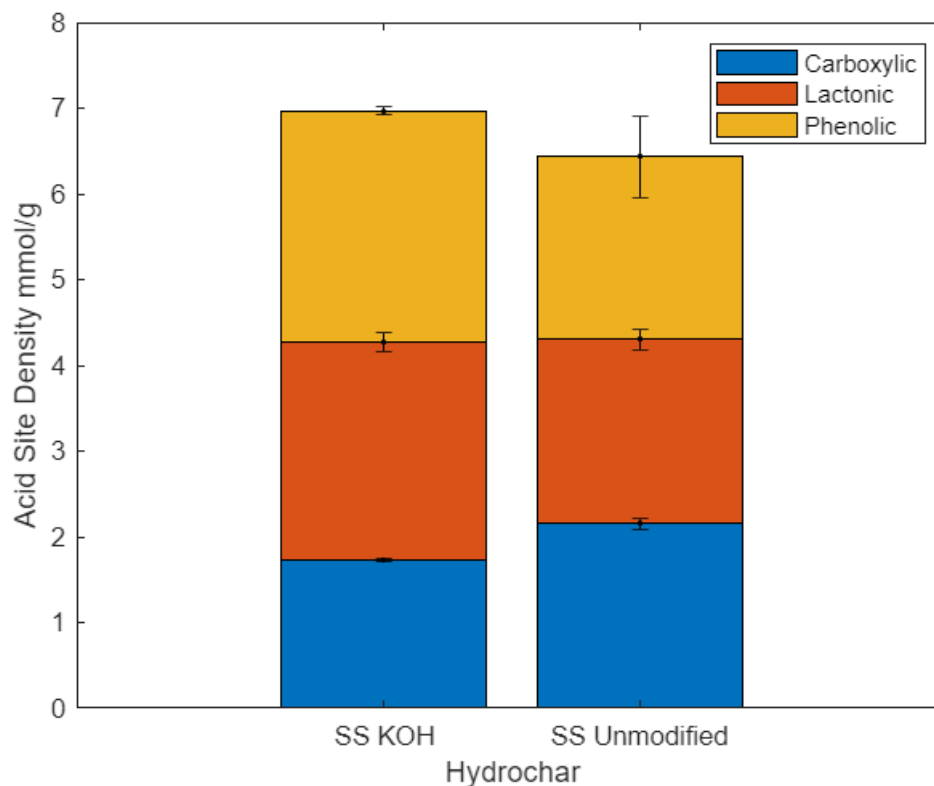


**Figure 11:** Acid Group Breakdown of Unmodified and KOH Activated SoMax Sewage Sludge Hydrochar Derived from Boehm Titration

The total acid site density of both samples is larger but on a similar scale to the designer hydrochar glucose, acrylic acid, glycine, and urea tested by Moran who followed the same method [65]. As seen in Figure 12 the total acid site density of sewage sludge hydrochar detected from Boehm titration is not consistent throughout the literature. It should be noted that it is difficult to directly compare Boehm titration results directly as there is a lack of standardization in technique [121]. However, the distribution of the acid sites detected is also inconstant throughout the models found in the literature.

**Table 2: Summary of Boehm Titration Results mmol/g**

Hydrochar	Carboxylic	Lactonic	Phenolic	Total	Base
SoMax Unmodified	2.14 ±0.07	2.54 ±0.12	2.70 ±0.03	7.38 ±0.32	0.39 ±0.12
SoMax KOH	1.73 ±0.02	2.15 ±0.12	2.13 ±0.48	6.01 ±0.62	0.17 ±0.02
Glucose [66]	0.9 ±0.1	1.3 ±0.3	3.0 ±0.5	5.2 ±0.4	-0.4 ±0.3
SS Literature Model 1 [122]	4.29	0.29	0.51	5.09	N/A
SS Literature Model 2 [123]	1.26	0.222	0.288	1.77	1.52
SS Literature Model 3 [124]	0.17	0.03	0.21	0.41	N/A

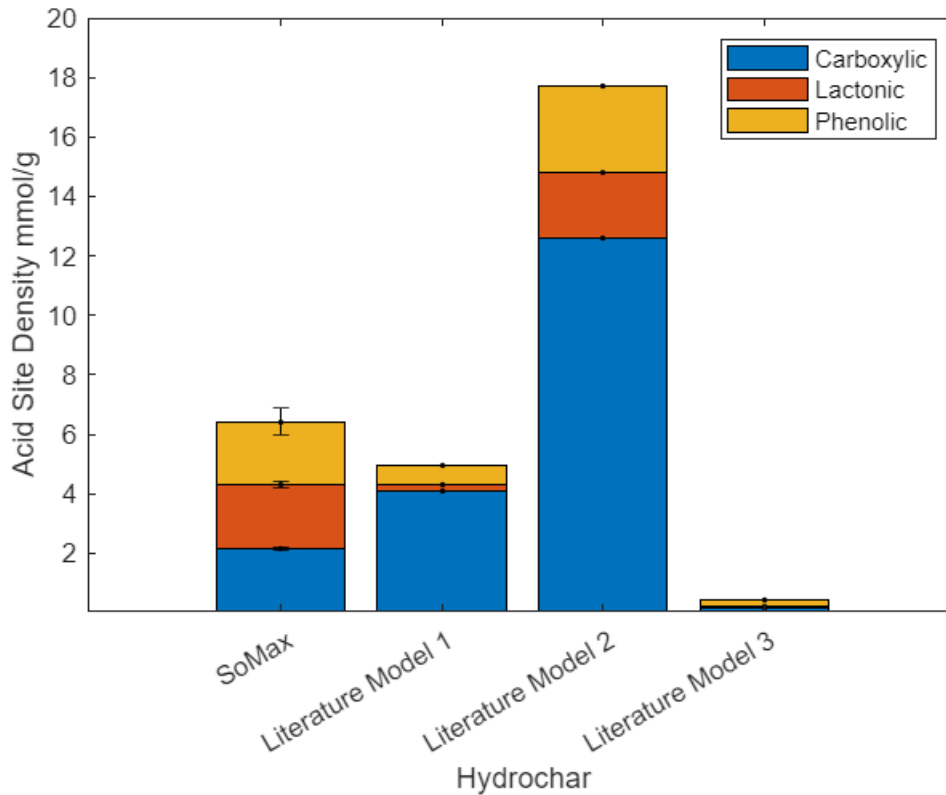


*Figure 12: Acid Group Breakdown of Unmodified Sewage Sludge Hydrochars from SoMax and Literature Derived from Boehm Titration [122], [123], [124]*

The titration results from the literature were derived from hydrochar produced using different process parameters, this was due to a lack of available published work on the topic. Boehm titration of hydrochar produced from the same feed but using different process parameters by He and Giannis [122] showed that acid site density and distribution were affected by process severity, but not to a degree that would explain the results shown in Figure 12. This suggests that the surface functionality of sewage sludge hydrochar highly varies depending on the sewage feedstock. The high ash content of the sewage hydrochar may also explain the high variation in detected acid site density as high ash content has been found to interfere with Boehm titration results [125]. The ash content from the literature sewage sludge hydrochar varied between 34-52% [122], [123], [124]. Pretreatment to lower the ash content of sewage sludge hydrochar should yield more reliable results [126].

The detected base site density in both samples was considerably lower than that of the acid site density. This is to be expected as HTC occurs in acidic conditions [43]. A higher base site density was detected in the KOH-activated hydrochar, which is easily explained by the activation process exposing the hydrochar to a strong base.

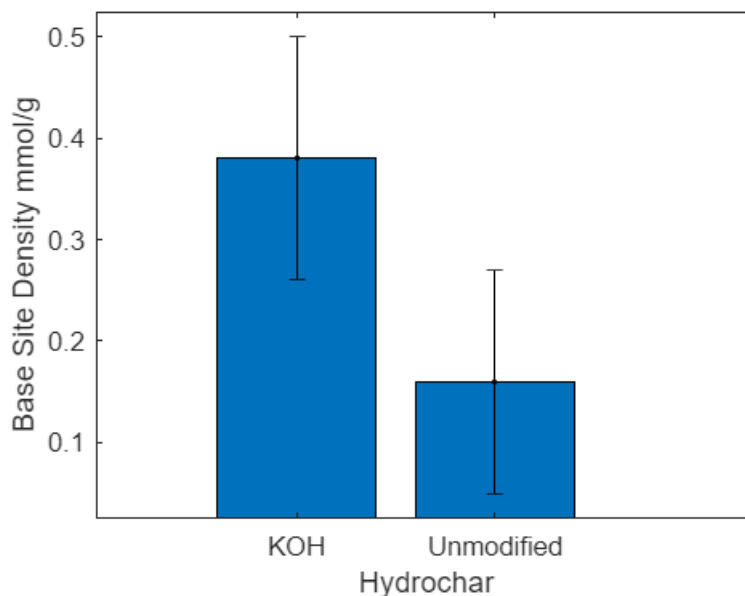


**Figure 13:** Base Site Density of Unmodified and KOH Activated SoMax Sewage Sludge Hydrochar Derived from Boehm Titration

Figure 14 shows the Raman spectra obtained from the unmodified SoMax Hydrochar baselined corrected and manually peak fit with 12-peak analysis protocol described by Brown [125] used the 12-peak fit to characterize glucose hydrochar, which we will use as a comparison as a pure feedstock source or hydrochar. The Raman spectra consist of many overlapping C-C bands due to the complex amorphous nature of hydrochar. Brown developed a 12-band model using glucose hydrochar that consists of G, D, Kekule (arene) /Furan, and several other less prominent bands [125]. The G and D bands are attributed to the asymmetric and symmetric arene ring C-C stretching vibrations respectively. Using this model Brown was able to reproduce the main features of the glucose hydrochar Raman spectrum. Using this same 12-peak model we manually fit the Raman spectra of the unmodified SoMax hydrochar using method 3 detailed by Brown which allowed for variation in the height of all 12 bands and the width of the 3 most

prominent bands, G 51.31%, D 34.46%, and Kekule/Furan 11.16%.

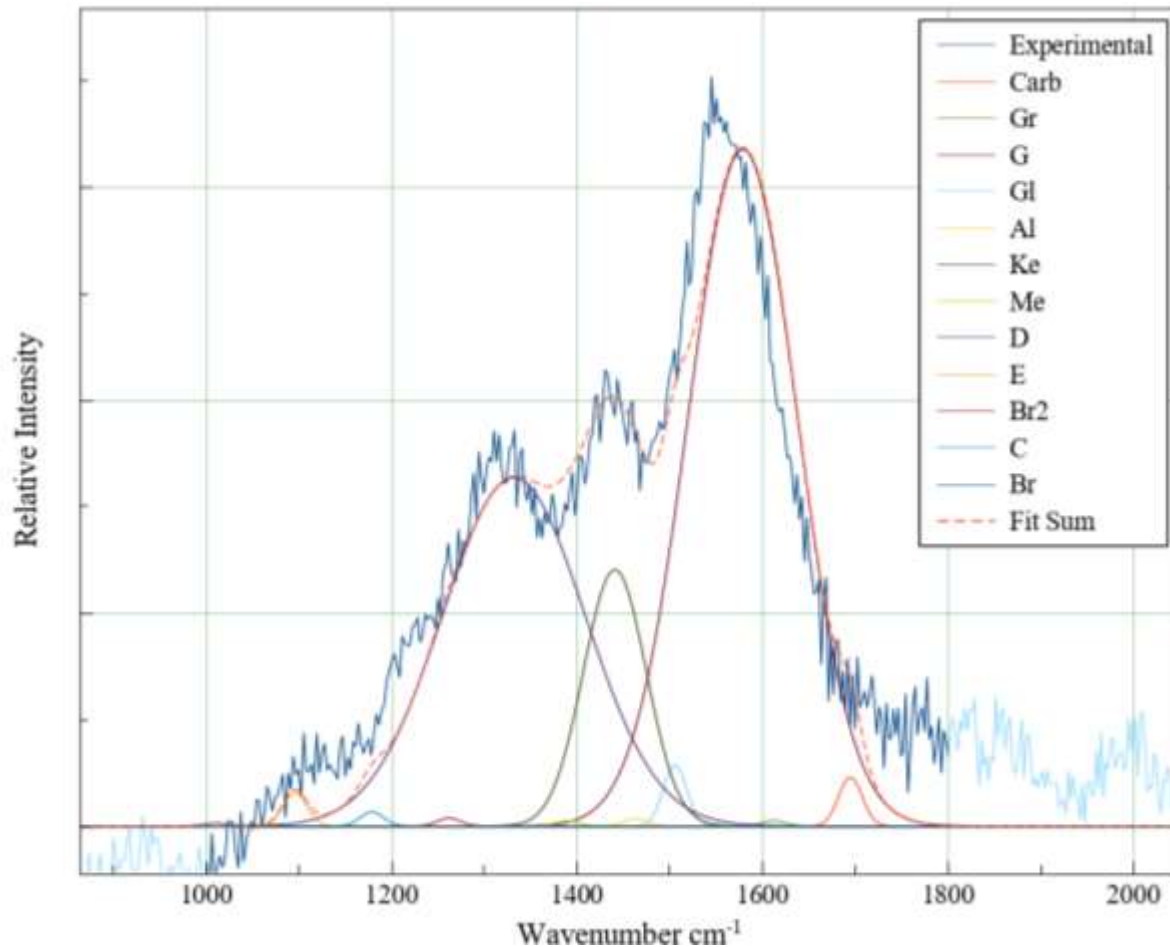


**Figure 14:** *Experimental Raman Spectra Sum Against Known Vibrational Bands of Glucose Hydrochar*

Brown's model when applied to the SoMax hydrochar gives an R2 of 0.95. Notably the most intense band G is shifted right in the model compared to experimental data. It is possible averaging several Raman spectra of the SoMax hydrochar would decrease this error. The model suggests that G, D, and Kekule/Furan bands are the most prominent features in the SoMax hydrochar with all other bands each accounting for <1% of the total area of the fit sum indicating a low concentration of these features in the structure. Table 3 provides a complete breakdown of

the relative intensities of peaks of the 12-peak fit model for the SoMax hydrochar compared to Glucose hydrochar.

*Table 3: Hydrochar Composition Features of SoMax and Glucose Hydrochar from Raman Spectra [124]*

<b>Band Name</b>	<b>Location cm<sup>-1</sup></b>	<b>Percent Area SoMax</b>	<b>Percent Area Glucose</b>
Carbonyl Band	1695	0.80	5.09
Gr Band	1612	0.087	1.43
G Band	1579	51.31	26.21
Gl Band	1506	0.99	9.2
Aliphatic mode	1463	0.12	0.00
Kekule/Furan	1441	11.16	9.56
Methyl Band	1390	0.085	9.50
D Band	1332	34.46	14.58
Ether	1096	0.54	4.17
Breathing model 2	1262	0.13	11.18
C-H wagging on rings	1179	0.23	11.18
Breathing model	1011	0.05	2.51

The D and G bands in the SoMax hydrochar are twice the area as the glucose hydrochar, suggesting that the SoMax hydrochar contains a relatively higher amount of arene rings. The Kekule/Furan band had similar intensities while all other bands were much less prominent in the SoMax hydrochar, such as the low intensity of the methyl band suggesting a lack of methyl groups. In addition, the relatively low areas of peaks from functional groups such as ether, and

carbonyl suggests less functionality of the SoMax hydrochar relative to the glucose hydrochar. This is inconsistent with results from Boehm titration and FTIR that indicated the SoMax sewage sludge hydrochar had a higher relative amount of surface functional groups. Raman spectroscopy does not indicate O-H bonds which are more important when discussing these functional groups and these inconsistencies can likely be attributed to a poor fit of Brown's model to the SoMax hydrochar. Averaging several SoMax hydrochar Raman spectra may help correct these inconsistencies.

### **Copper Adsorption**

Adsorption isotherms for both the activated and unmodified SoMax hydrochar can be seen in Figure 15. The unmodified hydrochar was found to have a max adsorption capacity of 22.6 mg Cu(II)/g-1. This is significantly higher adsorption capacity compared to the unmodified glucose hydrochar tested by Delahaye and Hobson which detected no Cu(II) adsorption [8]. It is still lower than the KOH-activated glucose hydrochar by Delahaye and Hobson which through single-point adsorption was found to be 40 mg Cu(II)/g-1. The KOH-activated SoMax hydrochar was determined to have a maximum adsorption capacity of 49.0 mg Cu(II)/g-1, an increase of 116%. This is comparable adsorption to sewage sludge hydrochar by Spataru, Rohan Jain which was measured to have an adsorption capacity of 18.6 and 38.5 mg Cu(II)/g-1 pre and post-KOH activation an increase of 107% [85].

The calculated adsorption capacity error was determined by measuring the equilibrium concentration of samples without hydrochar and was determined to be consistently around 20%. The largest source of error identified was imprecise measuring during dilutions. Micropipettes were used whenever possible but larger volumes e.g., 50 mL were poured by hand.

Implementing larger precision measuring tools could help to decrease the error in future experiments.

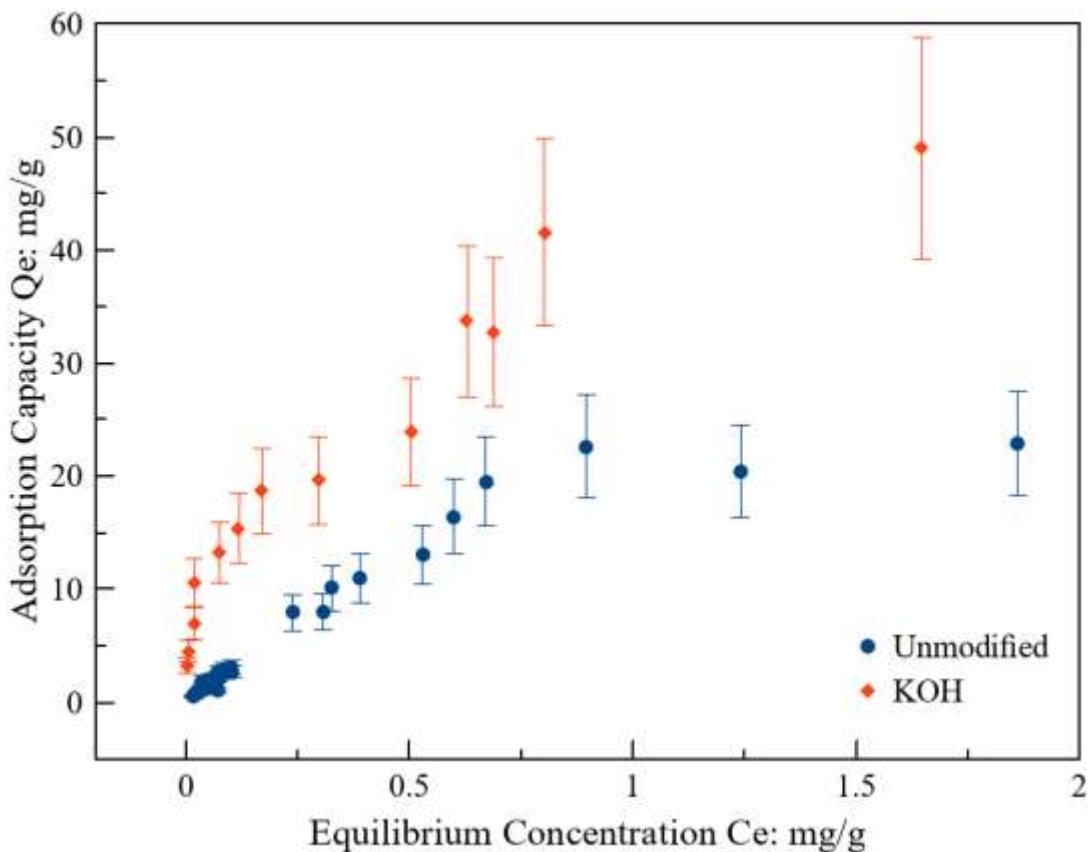


**Figure 15:** *Unmodified and KOH Activated Hydrochar Cu(II) adsorption Isotherm Derived from ICP-ms data*

The increased adsorption capacity detected by ICP-ms can be attributed to additional oxygenated surface groups, specifically hydroxyl groups detected by FTIR and Boehm Titration. Due to the lack of BET surface analysis and the inability of the XRF spectrometer to detect the presence of K, it is impossible to correlate the adsorption results to those properties of the hydrochar. Silica and iron oxide have independently been shown to have Cu(II) adsorption capabilities and due to the high relative amount of ash in the sample it is likely both materials contribute to total adsorption capacity of the hydrochar samples and shapes of the isotherms. Results from literature have shown iron oxides to have a Cu(II) adsorption capacity in the range

of 12.7 mg Cu(II)/g-1 [133] and Silica to be in the range of 2.17 mg Cu(II)/g-1 [134] [135].

Since the KOH modified hydrochar has a lower ash content and higher adsorption capacity than the unmodified hydrochar it would suggest that the involatile compounds in the sample contribute less to Cu(II) adsorption than the volatile ones.

Previous studies in literature have commonly fitted hydrochar Cu(II) adsorption data to Freundlich and Langmuir models, with Langmuir being the generally accepted best model to describe the adsorption process [85], [127], [128]. Langmuir adsorption assumes that adsorption occurs in a homogenous monolayer and there are no interactions between adjacent adsorbed molecules [130].

$$Q_e = Q_m * (K_l * C_e) / (1 + K_l * C_e)$$

***Equation 4: Langmuir Adsorption Model***

Equation 4 was used to construct the Langmuir models.  $K_l$  and  $Q_m$  were constants derived from plotting experimental values of  $C_e/Q_e$  vs  $C_e$ , where  $K_l$  is equal to the slope/intercept and  $Q_m$  is equal to  $1/\text{intercept}$ . Freundlich adsorption assumes heterogeneous multilayer adsorption and was modeled using Equation 5 [130].  $K_f$  and  $n$  are constants taken from plotting the natural log of experimental values of  $C_e$  vs the natural log of experimental values of  $Q_e$ , where  $n$  is  $1/\text{slope}$  and  $K_f$  equals  $\exp(\text{intercept})$ .

$$Q_e = K_f * C_e^{1/n}$$

***Equation 5: Freundlich Adsorption Model***

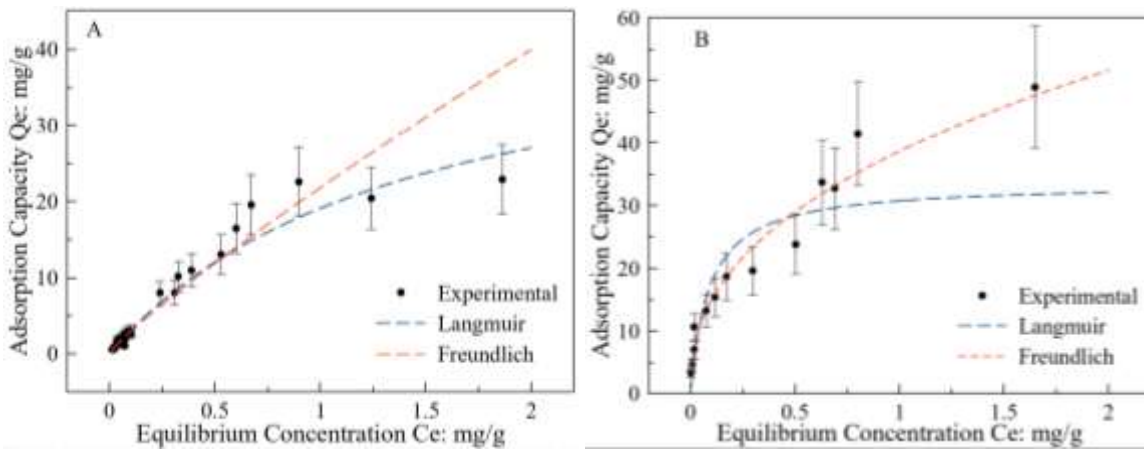


**Figure 16:** Langmuir and Freundlich Cu(II) Adsorption Models SoMax Hydrochar (A) Unmodified (B) KOH Activated

Between Langmuir and Freundlich, the Langmuir model fits the unmodified hydrochar better and Freundlich fits the activated hydrochar better, although neither model for either curve was able to fully represent the shape of the data. A full summary of the goodness of fit of all the fitting models used can be seen in Table 4. Akaike information criterion (AICc) values were calculated using equation 6 and were used to compare the relative goodness of fit of the models. AICc was used instead of AIC due to a low number of data points. Likely the cause of the different shapes of the isotherms is the increase in oxygenated surface sites shown by FTIR and Boehm titration. KOH activation created new Cu(II) binding sites that the Freundlich model is better able to represent. It is not possible to make claims on what effect a change in the surface area had on the isotherms as the BET surface area of either hydrochar was not determined. However, while an increase in surface area would theoretically increase the adsorption capacity it should have little effect on the shape of the isotherm aside from a positive shift in the Y-axis, as it would open more binding sites.

The decreased ash content likely had minor contributions to the changes in hydrochar isotherm shapes compared to the increase in functional groups, as the ash content in the KOH

hydrochar was still relatively high 41.6%. Notably however silica has been shown to exhibit Langmuir adsorption [134] while iron oxide adsorption has been shown to more closely follow a Freundlich adsorption model [133]. An elemental analysis could reveal how specifically the ash component changed post KOH treatment and the iron oxide to silica ratio. FTIR indicated a lower silica content while the band attributed to metal oxides was consistent between spectra. This suggests that the loss of silica was primarily responsible for the decrease in ash content. Since silica has a lower Cu(II) adsorption capacity than Iron Oxide on a per mass basis, it could also contribute to the higher detected adoption capacity of the KOH activated Hydrochar, as well as the better fit to the Freundlich model.

**Table 4: Summary of Goodness of Fit of Different Fitting Models**

<b>Model</b>	<b>Unmodified R<sup>2</sup></b>	<b>Unmodified AICc</b>	<b>KOH R<sup>2</sup></b>	<b>KOH AICc</b>
Langmuir	0.96	171	0.53	108
Freundlich	0.88	223	0.96	73
SIPS	0.94	206	0.89	109
Dual Site	0.93	198	0.98	68
Dual Site Interacting	0.92	234	0.88	155

$$AICc = n \ln \left( \frac{SSE}{n} \right) + 2k + \frac{2k(k+1)}{n-k-1} + n \ln(2\pi) + n$$

**Equation 6: Akaike Information Criterion Values; k Number of Parameter, n Sample Size [131]**

To better capture the shape of the isotherms the experimental data was fit against the SIPS model which is a combination of the Langmuir and Freundlich models, that is suitable for

describing heterogeneous adsorption [132]. The SIPS model had similar issues as the Langmuir model having a very similar shape, generally underpredicting adsorption capacities and an inability to model raises or dips in the curve.

$$Q_e = Q_m * (K_l * C_e)^n / ((1 + (K_l * C_e)^n))$$

**Equation 7: SIPS Adsorption Model [132]**

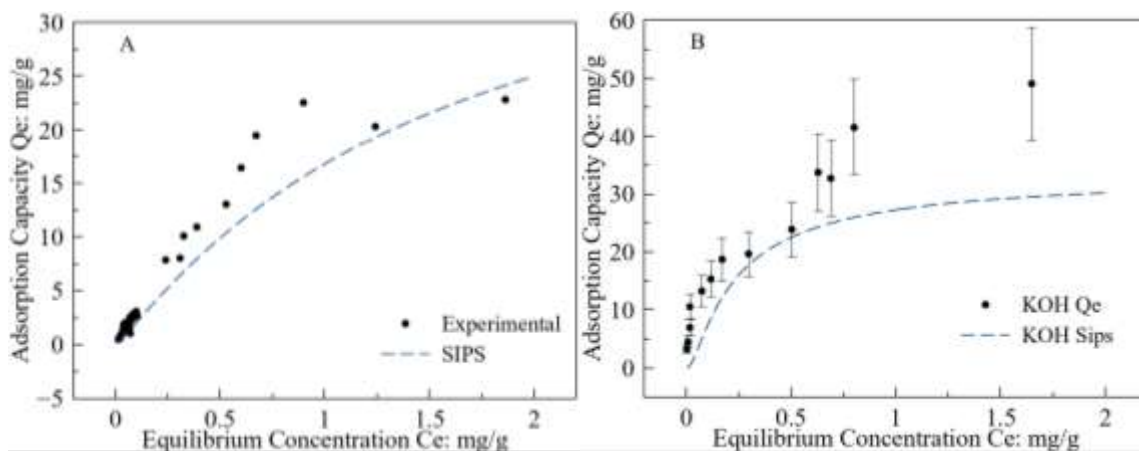


**Figure 17: SIPS Cu(II) Adsorption Model SoMax Hydrochar (A) Unmodified (B) KOH Activated**

It was observed that the Langmuir-based models fit both isotherms well at low concentrations but began to drift from experimental data at equilibrium concentrations above 0.53 and 0.29 mg Cu(II)/g-1 for unmodified and KOH activated respectively. Especially noticeable in the KOH-activated isotherm are the two areas of sharp increase followed by a section of leveling off. Individually these are the shapes typical of Langmuir' and to better capture the multisite adsorption a dual site Langmuir and dual site interacting Langmuir model were fit against the experimental data. The dual-site Langmuir model split the isotherm into 2 sections and modeled each as a separate Langmuir isotherm, while the interacting dual-site model was constructed

according to Equation 8. Constants  $Q_{m2}$ ,  $K_{l1}$ , and  $K_{l2}$  are derived the same as  $Q_m$  and  $K_l$  in the single site Langmuir Model but from the split isotherm sections.

$$Q_e = Q_{m2} * \left( \frac{K_{l1} * C_e}{1 + K_{l1} * C_e} \right) * \left( \frac{K_{l2} * C_e}{1 + K_{l2} * C_e} \right)$$

**Equation 8: Dual Site Interacting Langmuir Model**

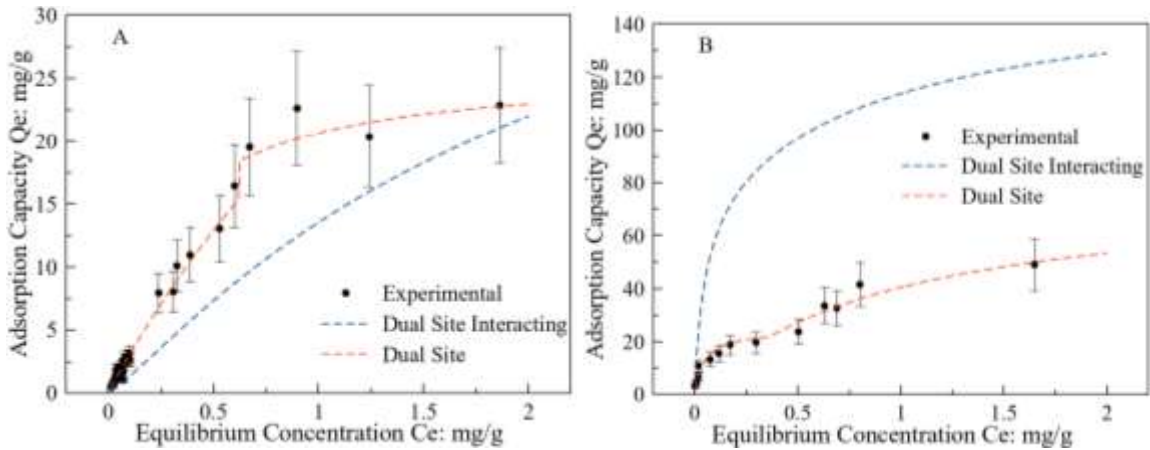


**Figure 18: Dual Site and Dual Site Interacting Cu(II) Adsorption Models SoMax Hydrochar (A) Unmodified (B) KOH Activated**

The dual site interacting model was found to have the worst fit out of any of the models for both hydrochar, underpredicting adsorption in the unmodified hydrochar and grossly overestimating the KOH-activated hydrochar. The noninteracting dual-site model was found to have the best fit for the activated hydrochar, and the second best fit for the unmodified hydrochar performing under the Langmuir model. This suggests that the activated hydrochar has two prominent binding sites while the unmodified hydrochar only has one prominent site. The secondary site is likely present in the unmodified hydrochar explaining inconsistencies in the Langmuir model just in a lower amount. Boehm titration data would suggest that the secondary site is hydroxyl groups, and the primary site is carboxyl groups, which is consistent with DFT

modeling by Gatsonis [101]. This also implies that the binding sites are not competitive and that one binding site is preferred over the other, with Cu(II) ions only binding to the second site when all the first are unavailable. The isotherms suggest that the carboxyl groups are the primary and preferred adsorption site as the first section of activated hydrochar  $C_e < 0.6$  mg/g shares a similar shape and adsorption capacity to that of the modified hydrochar relative to the second section  $> 0.6$  mg/g. The increased adsorption at a lower equilibrium concentration of the activated Hydrochar could potentially be explained by KOH deprotonation of the carboxyl groups as detailed in section 2.8.

Iron oxide/silica could also be responsible for one of the adsorption sites or simply be the cause for inconsistencies in between experimental data and the models. Lack of the distinct C=O carbonyl band in the FTIR spectra would suggest the former. It is also possible that carboxylate groups, possibly detected by FTIR are responsible for one of the adsorption sites. Comparison of further adsorption tests on both the calcined hydrochar and washed hydrochar that have a lower ash content would allow for better determination in what role both play in the overall material Cu(II) adsorption.

All of these models are only based on adsorption data of copper solutions at equilibrium data less than 2 mg Cu(II)/g solution and are of questionable use at higher concentrations. If the dual site model is believed to be accurate the adsorption capacity of the unmodified SoMax hydrochar should not exceed 26.0 mg Cu(II)/g while the KOH-activated hydrochar has a max adsorption of 78.0 mg Cu(II)/g at high equilibrium concentrations  $> 2$  mg Cu(II)/g solution. These claims are based on the assumption that the isotherms continue with the same adsorption pattern and that Cu(II) does not bind to the Hydrochar another surface site once the previous two are full.

## Conclusions & Recommendations

The SoMax sewage sludge hydrochar was found to be an effective adsorbent of Cu(II) without secondary treatment, with KOH further increasing the adsorption capacity. The adsorption ability of the hydrochar was attributed to oxygenated functional groups specifically carboxylic groups which was expected. The increase in the activated hydrochar adsorption capacity was attributed to an increase in oxygenated functional groups in particular hydroxyl groups detected by FTIR and Boehm titration, as well as a decrease in the ash content specifically silica. The unmodified hydrochar most closely fits a Langmuir adsorption model and the KOH activated hydrochar fitting a dual site Langmuir model. Inconsistencies in Boehm titration and FTIR lead to difficulties in attributing the adsorption sites.

For future work, it is recommended an elemental and BET surface analysis of the hydrochar be performed to determine if KOH activated led to a detectable higher amount of potassium in the hydrochar and if surface area increased. Since FTIR data had no clear alkali carboxylate bands, an elemental analysis would help to determine if the acid site deprotonation theory proposed by Delahaye and Hobson. It is also recommended that the Boehm titration experiments be repeated with hydrochar that has been treated to lower the ash content. Many of the conclusions were derived from the Boehm titration results and high ash content has been found to interfere with Boehm titration results. Other experimental results are less impacted by a high ash content as they characterized the entire material, and it is unlikely hydrochar will undergo additional treatment on the commercial scale for economic reasons. Characterization of the SoMax hydrochar revealed it to have many similarities to glucose hydrochar suggesting a related structure.

Further adsorption tests may need to be performed on hydrochar with a lower ash content and the ash content itself to better understand to what degree iron oxide and silica participated in Cu(II) adsorption, and if the ash content was substantially lowered or removed entirely if it would drastically alter the adsorption isotherm and adsorption capacity. Additional future work may also include testing the adsorption capacity of the hydrochar for additional heavy metals such as lead or testing the adsorption of several compounds at once such as the Cu(II) ions and methyl blue as wastewater is not homogenous and often contains multiple contaminants. It will be important to see if different compounds bind to the same or different sites especially as KOH has been shown to increase the adsorption capacity of both methyl blue and Cu(II). Finally, the adsorption capacity can be compared to commercially available filter materials such as activated carbon to determine the economic viability of implementation.

## References

1. Venkatesan AK, Done HY, Halden RU. United States National Sewage Sludge
2. Tasca, A. L., Puccini, M., Gori, R., Corsi, I., Galletti, A. M. R., & Vitolo, S. (2019). Hydrothermal carbonization of sewage sludge: A critical analysis of process severity, hydrochar properties and environmental implications. In *Waste Management* (Vol. 93, pp. 1–13).
3. Kacprzak, M., Neczaj, E., Fijałkowski, K., Grobelak, A., Grosser, A., Worwag, M., Rorat, A., Brattebo, H., Almås, Å., & Singh, B. R. (2017). Sewage sludge disposal strategies for sustainable development. In *Environmental Research* (Vol. 156, pp. 39–46).
4. Kang, S., Li, X., Fan, J., & Chang, J. (2012). Characterization of Hydrochars Produced by Hydrothermal Carbonization of Lignin, Cellulose, <scpd/>-Xylose, and Wood Meal. In *Industrial & Engineering Chemistry Research* (Vol. 51, Issue 26, pp. 9023–9031).
5. Masoumi, S., Borugadda, V. B., Nanda, S., & Dalai, A. K. (2021). Hydrochar: A Review on Its Production Technologies and Applications. In *Catalysts* (Vol. 11, Issue 8, p. 939).
6. Romano, P., Stampone, N., & Di Giacomo, G. (2023). Evolution and Prospects of Hydrothermal Carbonization. In *Energies* (Vol. 16, Issue 7, p. 3125).
7. Kambo, H. S., & Dutta, A. (2015). A comparative review of biochar and hydrochar in terms of production, physico-chemical properties and applications. In *Renewable and Sustainable Energy Reviews* (Vol. 45, pp. 359–378).
8. Delahaye, L., Hobson, J. T., Rando, M. P., Sweeney, B., Brown, A. B., Tompsett, G. A., Ates, A., Deskins, N. A., & Timko, M. T. (2020). Experimental and Computational Evaluation of Heavy Metal Cation Adsorption for Molecular Design of Hydrothermal Char. In *Energies* (Vol. 13, Issue 16, p. 4203).
9. Liang, Y., Xu, D., Feng, P., Hao, B., Guo, Y., & Wang, S. (2021). Municipal sewage sludge incineration and its air pollution control. In *Journal of Cleaner Production* (Vol. 295, p. 126456).
10. Wang, M.-J. (1997). Land application of sewage sludge in China. In *Science of The Total Environment* (Vol. 197, Issues 1–3, pp. 149–160).
11. Hong, J., Hong, J., Otaki, M., & Jolliet, O. (2009). Environmental and economic life cycle assessment for sewage sludge treatment processes in Japan. In *Waste Management* (Vol. 29, Issue 2, pp. 696–703).
12. US EPA, O. (2020, March 2). *Biosolids Laws and Regulations*. [Www.epa.gov. https://www.epa.gov/biosolids/biosolids-laws-and-regulations#how](https://www.epa.gov/biosolids/biosolids-laws-and-regulations#how)
13. *Sewage sludge*. (2023, March 8). [Environment.ec.europa.eu. https://environment.ec.europa.eu/topics/waste-and-recycling/sewage-sludge\\_en#:~:text=The%20Directive%20on%20sewage%20sludge](https://environment.ec.europa.eu/topics/waste-and-recycling/sewage-sludge_en#:~:text=The%20Directive%20on%20sewage%20sludge)

14. US EPA, O. (n.d.). *EPA History: Ocean Dumping Ban Act of 1988*. Www.epa.gov. <https://www.epa.gov/archive/epa/aboutepa/epa-history-ocean-dumping-ban-act-1988.html>
15. US EPA, O. (2016, July 13). *Basic Information about Biosolids*. US EPA. <https://www.epa.gov/biosolids/basic-information-about-biosolids#basics>
16. Novak, J. T. (2006). Dewatering of Sewage Sludge. In *Drying Technology* (Vol. 24, Issue 10, pp. 1257–1262).
17. Masmoudi, A., Ben Sik Ali, A., Dhaouadi, H. *et al.* Comparison Between Two Solar Drying Techniques of Sewage Sludge: Draining Solar Drying and Drying Bed. *Waste Biomass Valor* **12**, 4089–4102 (2021).
18. Kelessidis, A., & Stasinakis, A. S. (2012). Comparative study of the methods used for treatment and final disposal of sewage sludge in European countries. In *Waste Management* (Vol. 32, Issue 6, pp. 1186–1195).
19. O’Kelly, B. C. (2005). Sewage Sludge to Landfill: Some Pertinent Engineering Properties. In *Journal of the Air & Waste Management Association* (Vol. 55, Issue 6, pp. 765–771).
20. Tytła, M. (2019). Assessment of Heavy Metal Pollution and Potential Ecological Risk in Sewage Sludge from Municipal Wastewater Treatment Plant Located in the Most Industrialized Region in Poland—Case Study. In *International Journal of Environmental Research and Public Health* (Vol. 16, Issue 13, p. 2430).
21. Singh, R. P., Singh, P., Ibrahim, M. H., & Hashim, R. (2011). Land Application of Sewage Sludge: Physicochemical and Microbial Response. In *Reviews of Environmental Contamination and Toxicology* (pp. 41–61).
22. Geng, H., Xu, Y., Zheng, L., Gong, H., Dai, L., & Dai, X. (2020). An overview of removing heavy metals from sewage sludge: Achievements and perspectives. In *Environmental Pollution* (Vol. 266, p. 115375).
23. Zhang, X., Wang, X., & Wang, D. (2017). Immobilization of Heavy Metals in Sewage Sludge during Land Application Process in China: A Review. In *Sustainability* (Vol. 9, Issue 11, p. 2020).
24. Hanay, O., Hasar, H., & Kocer, N. N. (2009). Effect of EDTA as washing solution on removing of heavy metals from sewage sludge by electrokinetic. In *Journal of Hazardous Materials* (Vol. 169, Issues 1–3, pp. 703–710).
25. Shi, W., Liu, C., Ding, D., Lei, Z., Yang, Y., Feng, C., & Zhang, Z. (2013). Immobilization of heavy metals in sewage sludge by using subcritical water technology. In *Bioresource Technology* (Vol. 137, pp. 18–24).
26. Amir, S.; Hafidi, M.; Merlina, G.; Revel, J.C. Sequential extraction of heavy metals during composting of sewage sludge. *Chemosphere* 2005, *59*, 801–810.
27. Hsiau, P.C.; Lo, S.L. Effects of lime treatment on fractionation and extractabilities of heavy metals in sewage sludge. *J. Environ. Sci. Health Part A* **1997**, *32*, 2521–2536.

28. Sajwan, K. S., Paramasivam, S., Alva, A. K., Adriano, D. C., & Hooda, P. S. (2003). Assessing the feasibility of land application of fly ash, sewage sludge and their mixtures. In *Advances in Environmental Research* (Vol. 8, Issue 1, pp. 77–91).
29. Antoniadis, V., Damalidis, K., & Dimirkou, A. (2011). Availability of Cu and Zn in an acidic sludge-amended soil as affected by zeolite application and liming. In *Journal of Soils and Sediments* (Vol. 12, Issue 3, pp. 396–401).
30. Cao, X., Liang, Y., Zhao, L., & Le, H. (2012). Mobility of Pb, Cu, and Zn in the phosphorus-amended contaminated soils under simulated landfill and rainfall conditions. In *Environmental Science and Pollution Research* (Vol. 20, Issue 9, pp. 5913–5921).
31. Samolada, M. C., & Zabaniotou, A. A. (2014). Comparative assessment of municipal sewage sludge incineration, gasification and pyrolysis for a sustainable sludge-to-energy management in Greece. In *Waste Management* (Vol. 34, Issue 2, pp. 411–420).
32. Cai, L., Krafft, T., Chen, T.-B., Gao, D., & Wang, L. (2016). Structure modification and extracellular polymeric substances conversion during sewage sludge biodrying process. In *Bioresource Technology* (Vol. 216, pp. 414–421).
33. Wang, W., Luo, Y. & Qiao, W. Possible solutions for sludge dewatering in China. *Front. Environ. Sci. Eng. China* **4**, 102–107 (2010). <https://doi.org/10.1007/s11783-010-0001-z>
34. Ma, J., Zhang, L., & Li, A. (2016). Energy-efficient co-biodrying of dewatered sludge and food waste: Synergistic enhancement and variables investigation. In *Waste Management* (Vol. 56, pp. 411–422).
35. Yang, B., Zhang, L., & Jahng, D. (2013). Importance of Initial Moisture Content and Bulking Agent for Biodrying Sewage Sludge. In *Drying Technology* (Vol. 32, Issue 2, pp. 135–144).
36. EPA. (2018). *Nitrogen Oxides Control Regulations / Ozone Control Strategies / Ground-level Ozone / New England / US EPA*. Epa.gov. <https://www3.epa.gov/region1/airquality/nox.html>
37. US EPA, O. (2016, September 16). *Sulfur Dioxide (SO<sub>2</sub>) Primary Air Quality Standards*. Wwww.epa.gov. <https://www.epa.gov/naaqs/sulfur-dioxide-so2-primary-air-quality-standards>
38. Hitzl, M., Corma, A., Pomares, F., & Renz, M. (2015). The hydrothermal carbonization (HTC) plant as a decentral biorefinery for wet biomass. In *Catalysis Today* (Vol. 257, pp. 154–159).
39. Yan, Y., Ma, X., Cao, W., Zhang, X., Zhou, J., Liu, Q., & Qian, G. (2018). Identifying the reducing capacity of biomass derived hydrochar with different post-treatment methods. In *Science of The Total Environment* (Vol. 643, pp. 486–495).
40. Gascó, G., Paz-Ferreiro, J., Álvarez, M. L., Saa, A., & Méndez, A. (2018). Biochars and hydrochars prepared by pyrolysis and hydrothermal carbonisation of pig manure. In *Waste Management* (Vol. 79, pp. 395–403).
41. Khan, M. A., Hameed, B. H., Siddiqui, M. R., Alothman, Z. A., & Alsohaimi, I. H. (2022). Comparative Investigation of the Physicochemical Properties of Chars Produced

- by Hydrothermal Carbonization, Pyrolysis, and Microwave-Induced Pyrolysis of Food Waste. In *Polymers* (Vol. 14, Issue 4, p. 821).
42. Mendoza Martinez, C. L., Sermyagina, E., Saari, J., Silva de Jesus, M., Cardoso, M., Matheus de Almeida, G., & Vakkilainen, E. (2021). Hydrothermal carbonization of lignocellulosic agro-forest based biomass residues. In *Biomass and Bioenergy* (Vol. 147, p. 106004).
  43. Funke, A., & Ziegler, F. (2010). Hydrothermal carbonization of biomass: A summary and discussion of chemical mechanisms for process engineering. In *Biofuels, Bioproducts and Biorefining* (Vol. 4, Issue 2, pp. 160–177).
  44. Libra, J. A., Ro, K. S., Kammann, C., Funke, A., Berge, N. D., Neubauer, Y., Titirici, M.-M., Fühner, C., Bens, O., Kern, J., & Emmerich, K.-H. (2011). Hydrothermal carbonization of biomass residuals: a comparative review of the chemistry, processes and applications of wet and dry pyrolysis. In *Biofuels* (Vol. 2, Issue 1, pp. 71–106).
  45. Czerwińska, K., Śliz, M., & Wilk, M. (2022). Hydrothermal carbonization process: Fundamentals, main parameter characteristics and possible applications including an effective method of SARS-CoV-2 mitigation in sewage sludge. A review. In *Renewable and Sustainable Energy Reviews* (Vol. 154, p. 111873).
  46. Heidari, M., Dutta, A., Acharya, B., & Mahmud, S. (2019). A review of the current knowledge and challenges of hydrothermal carbonization for biomass conversion. In *Journal of the Energy Institute* (Vol. 92, Issue 6, pp. 1779–1799).
  47. Brunner, G. (2009). Near critical and supercritical water. Part I. Hydrolytic and hydrothermal processes. In *The Journal of Supercritical Fluids* (Vol. 47, Issue 3, pp. 373–381).
  48. Xiao, L.-P., Shi, Z.-J., Xu, F., & Sun, R.-C. (2012). Hydrothermal carbonization of lignocellulosic biomass. In *Bioresource Technology* (Vol. 118, pp. 619–623).
  49. Pauline, A. L., & Joseph, K. (2020). Hydrothermal carbonization of organic wastes to carbonaceous solid fuel – A review of mechanisms and process parameters. In *Fuel* (Vol. 279, p. 118472).
  50. Guo, S., Dong, X., Wu, T., & Zhu, C. (2016). Influence of reaction conditions and feedstock on hydrochar properties. In *Energy Conversion and Management* (Vol. 123, pp. 95–103).
  51. Khan, N., Mohan, S., & Dinesha, P. (2021). Regimes of hydrochar yield from hydrothermal degradation of various lignocellulosic biomass: A review. In *Journal of Cleaner Production* (Vol. 288, p. 125629).
  52. Ghanim, B. M., Kwapinski, W., & Leahy, J. J. (2017). Hydrothermal carbonisation of poultry litter: Effects of initial pH on yields and chemical properties of hydrochars. In *Bioresource Technology* (Vol. 238, pp. 78–85).
  53. Raja, P. M. V., & Barron, A. R. (2022, August 28). 2.3: *Bet surface area analysis of nanoparticles*. *Chemistry LibreTexts*.

54. Hazra, B., Vishal, V., & Singh, D. P. (2020). Applicability of Low-Pressure CO<sub>2</sub> and N<sub>2</sub> Adsorption in Determining Pore Attributes of Organic-Rich Shales and Coals. In *Energy & Fuels* (Vol. 35, Issue 1, pp. 456–464)
55. Oickle, A. M., Goertzen, S. L., Hopper, K. R., Abdalla, Y. O., & Andreas, H. A. (2010). Standardization of the Boehm titration: Part II. Method of agitation, effect of filtering and dilute titrant. In *Carbon* (Vol. 48, Issue 12, pp. 3313–3322).
56. Raja, P. M. V., & Barron, A. R. (2022b, August 28). *4.3: Raman spectroscopy. Chemistry LibreTexts.*
57. Das, A., & Guo, H. (2022). Raman spectroscopy. In *Reference Module in Earth Systems and Environmental Sciences*
58. Brown, A. B., Tompsett, G. A., Partopour, B., Deskins, N. A., & Timko, M. T. (2020). Hydrochar structural determination from artifact-free Raman analysis. In *Carbon* (Vol. 167, pp. 378–387).
59. University of Alberta. (n.d.). *How XRD works – EAS X-ray diffraction laboratory – University of Alberta.*
60. University of Pennsylvania. (2018, February 28). *XRD basics.* Department of Physics and Astronomy.
61. Bruker. (n.d.). *How does XRF work? High-Value Life Science and Material Research and Diagnostics Solutions | Bruker.*
62. *XRF Web Seminar Module 2 – Basic XRF Concepts Module 2: Basic XRF Concepts.* (2008). [https://clu-in.org/conf/tio/xrf\\_080408/prez/XRF\\_02pdf.pdf](https://clu-in.org/conf/tio/xrf_080408/prez/XRF_02pdf.pdf)
63. Elemental Analysis Core. (n.d.). *ICP-MS as a technique.* OHSU | Healing Begins with Discovery.
64. Wilschefski, S., & Baxter, M. (2019). Inductively Coupled Plasma Mass Spectrometry: Introduction to Analytical Aspects. In *Clinical Biochemist Reviews* (Vol. 40, Issue 3, pp. 115–133).
65. Moran, M. (2021). *Comparative Study of Experimental and Modeled Hydrochar Surface Properties.* : Worcester Polytechnic Institute.
66. Chuntanapum, A., & Matsumura, Y. (2009). Formation of Tarry Material from 5-HMF in Subcritical and Supercritical Water. In *Industrial & Engineering Chemistry Research* (Vol. 48, Issue 22, pp. 9837–9846).
67. Falco, C., Perez Caballero, F., Babonneau, F., Gervais, C., Laurent, G., Titirici, M.-M., & Baccile, N. (2011). Hydrothermal Carbon from Biomass: Structural Differences between Hydrothermal and Pyrolyzed Carbons via <sup>13</sup>C Solid State NMR. In *Langmuir* (Vol. 27, Issue 23, pp. 14460–14471).
68. Zhang, Z., Yang, J., Qian, J., Zhao, Y., Wang, T., & Zhai, Y. (2021). Biowaste hydrothermal carbonization for hydrochar valorization: Skeleton structure, conversion pathways and clean biofuel applications. In *Bioresource Technology* (Vol. 324, p. 124686).

69. Sevilla, M., & Fuertes, A. B. (2009). The production of carbon materials by hydrothermal carbonization of cellulose. In *Carbon* (Vol. 47, Issue 9, pp. 2281–2289).
70. Wang, C., Zhu, W., & Fan, X. (2021). Char derived from sewage sludge of hydrothermal carbonization and supercritical water gasification: Comparison of the properties of two chars. In *Waste Management* (Vol. 123, pp. 88–96).
71. Peng, C., Zhai, Y., Zhu, Y., Wang, T., Xu, B., Wang, T., Li, C., & Zeng, G. (2017). Investigation of the structure and reaction pathway of char obtained from sewage sludge with biomass wastes, using hydrothermal treatment. In *Journal of Cleaner Production* (Vol. 166, pp. 114–123).
72. Saha, N., Saba, A., & Reza, M. T. (2019). Effect of hydrothermal carbonization temperature on pH, dissociation constants, and acidic functional groups on hydrochar from cellulose and wood. In *Journal of Analytical and Applied Pyrolysis* (Vol. 137, pp. 138–145).
73. Nzediegwu, C., Naeth, M. A., & Chang, S. X. (2021). Carbonization temperature and feedstock type interactively affect chemical, fuel, and surface properties of hydrochars. In *Bioresource Technology* (Vol. 330, p. 124976).
74. Danso-Boateng, E., Ross, A.B., Mariner, T. *et al.* Hydrochars produced by hydrothermal carbonisation of seaweed, coconut shell and oak: effect of processing temperature on physicochemical adsorbent characteristics. *SN Appl. Sci.* **4**, 203 (2022).
75. Urbaniak, L. (2020). *Waste to Products: Hydrothermal Carbonization and Activation of Sewage Sludge for a Circular Economy Analyzed Through a Whole Systems Perspective*: Villanova University.
76. Leng, L., Xiong, Q., Yang, L., Li, H., Zhou, Y., Zhang, W., Jiang, S., Li, H., & Huang, H. (2021). An overview on engineering the surface area and porosity of biochar. In *Science of The Total Environment* (Vol. 763, p. 144204).
77. Lachos-Perez, D., César Torres-Mayanga, P., Abaide, E. R., Zabet, G. L., & De Castilhos, F. (2022). Hydrothermal carbonization and Liquefaction: differences, progress, challenges, and opportunities. In *Bioresource Technology* (Vol. 343, p. 126084).
78. Ren, S., Usman, M., Tsang, D. C. W., O-Thong, S., Angelidaki, I., Zhu, X., Zhang, S., & Luo, G. (2020). Hydrochar-Facilitated Anaerobic Digestion: Evidence for Direct Interspecies Electron Transfer Mediated through Surface Oxygen-Containing Functional Groups. In *Environmental Science & Technology* (Vol. 54, Issue 9, pp. 5755–5766).
79. Huang, H., Niu, Z., Shi, R., Tang, J., Lv, L., Wang, J., & Fan, Y. (2020). Thermal oxidation activation of hydrochar for tetracycline adsorption: the role of oxygen concentration and temperature. In *Bioresource Technology* (Vol. 306, p. 123096).
80. Zhu, X., Li, C., Li, J., Xie, B., Lü, J., & Li, Y. (2018). Thermal treatment of biochar in the air/nitrogen atmosphere for developed mesoporosity and enhanced adsorption to tetracycline. In *Bioresource Technology* (Vol. 263, pp. 475–482).

81. Diaz, E., Sanchis, I., Coronella, C. J., & Mohedano, A. F. (2022). Activated Carbons from Hydrothermal Carbonization and Chemical Activation of Olive Stones: Application in Sulfamethoxazole Adsorption. In *Resources* (Vol. 11, Issue 5, p. 43).
82. Zhang, X., Gao, B., Fang, J., Zou, W., Dong, L., Cao, C., Zhang, J., Li, Y., & Wang, H. (2019). Chemically activated hydrochar as an effective adsorbent for volatile organic compounds (VOCs). In *Chemosphere* (Vol. 218, pp. 680–686).
83. Oumabady, S., Selvaraj, P.S., Periasamy, K. *et al.* Kinetic and isotherm insights of Diclofenac removal by sludge derived hydrochar. *Sci Rep* **12**, 2184 (2022).
84. Spataru, A., Jain, R., Chung, J. W., Gerner, G., Krebs, R., & Lens, P. N. L. (2016). Enhanced adsorption of orthophosphate and copper onto hydrochar derived from sewage sludge by KOH activation. In *RSC Advances* (Vol. 6, Issue 104, pp. 101827–101834).
85. González, B., & Manyà, J. J. (2020). Activated olive mill waste-based hydrochars as selective adsorbents for CO<sub>2</sub> capture under postcombustion conditions. In *Chemical Engineering and Processing - Process Intensification* (Vol. 149, p. 107830).
86. Román, S., Valente Nabais, J. M., Ledesma, B., González, J. F., Laginhas, C., & Titirici, M. M. (2013). Production of low-cost adsorbents with tunable surface chemistry by conjunction of hydrothermal carbonization and activation processes. In *Microporous and Mesoporous Materials* (Vol. 165, pp. 127–133).
87. Bargmann, I., Rillig, M. C., Kruse, A., Greef, J., & Kücke, M. (2013). Effects of hydrochar application on the dynamics of soluble nitrogen in soils and on plant availability. In *Journal of Plant Nutrition and Soil Science* (Vol. 177, Issue 1, pp. 48–58).
88. Fei, Y., Zhao, D., Cao, Y., Huot, H., Tang, Y., Zhang, H., & Xiao, T. (2019). Phosphorous Retention and Release by Sludge-Derived Hydrochar for Potential Use as a Soil Amendment. In *Journal of Environmental Quality* (Vol. 48, Issue 2, pp. 502–509).
89. Bona, D., Bertoldi, D., Borgonovo, G., Mazzini, S., Ravasi, S., Silvestri, S., Zaccone, C., Giannetta, B., & Tambone, F. (2023). Evaluating the potential of hydrochar as a soil amendment. In *Waste Management* (Vol. 159, pp. 75–83).
90. Karatas, O., Khataee, A., & Kalderis, D. (2022). Recent progress on the phytotoxic effects of hydrochars and toxicity reduction approaches. In *Chemosphere* (Vol. 298, p. 134357).
91. Wu, Y., Hou, P., Guo, Z. *et al.* Raw material of water-washed hydrochar was critical for the mitigation of GHGI in infertile paddy soil: a column experiment. *Biochar* **3**, 381–390 (2021).
92. Puccini, M., Ceccarini, L., Antichi, D., Seggiani, M., Tavarini, S., Hernandez Latorre, M., & Vitolo, S. (2018). Hydrothermal Carbonization of Municipal Woody and Herbaceous Prunings: Hydrochar Valorisation as Soil Amendment and Growth Medium for Horticulture. In *Sustainability* (Vol. 10, Issue 3, p. 846).
93. Islam, M.A., Limon, M.S.H., Romić, M. *et al.* Hydrochar-based soil amendments for agriculture: a review of recent progress. *Arab J Geosci* **14**, 102 (2021).

94. Zhang, Z., Zhu, Z., Shen, B., & Liu, L. (2019). Insights into biochar and hydrochar production and applications: A review. In *Energy* (Vol. 171, pp. 581–598).
95. Yan, W., Hoekman, S. K., Broch, A., & Coronella, C. J. (2014). Effect of hydrothermal carbonization reaction parameters on the properties of hydrochar and pellets. In *Environmental Progress & Sustainable Energy* (Vol. 33, Issue 3, pp. 676–680).
96. Wang, Q., Wu, S., Cui, D., Zhou, H., Wu, D., Pan, S., Xu, F., & Wang, Z. (2022). Co-hydrothermal carbonization of organic solid wastes to hydrochar as potential fuel: A review. In *Science of The Total Environment* (Vol. 850, p. 158034).
97. Khan, M. A., Hameed, B. H., Siddiqui, M. R., Alothman, Z. A., & Alsohaimi, I. H. (2022). Hydrothermal Conversion of Food Waste to Carbonaceous Solid Fuel—A Review of Recent Developments. In *Foods* (Vol. 11, Issue 24, p. 4036).
98. huang, X., Song, Y., Zhan, H., Yin, X., & Wu, C. (2020). Gasification performance of biowaste-derived hydrochar: The properties of products and the conversion processes. In *Fuel* (Vol. 260, p. 116320).
99. Iwuozor, K.O., Abdullahi, T.A., Ogunfowora, L.A. *et al.* Mitigation of levofloxacin from aqueous media by adsorption: a review. *Sustain. Water Resour. Manag.* **7**, 100 (2021).
100. Ighalo, J. O., Rangabhashiyam, S., Dulta, K., Umeh, C. T., Iwuozor, K. O., Aniagor, C. O., Eshiemogie, S. O., Iwuchukwu, F. U., & Igwegbe, C. A. (2022). Recent advances in hydrochar application for the adsorptive removal of wastewater pollutants. In *Chemical Engineering Research and Design* (Vol. 184, pp. 419–456).
101. Gatsonis, A. (2022). *Investigation of Heavy Metal Adsorption to Hydrothermal Char* . : Worcester Polytechnic Institute.
102. Sun, K., Tang, J., Gong, Y. *et al.* Characterization of potassium hydroxide (KOH) modified hydrochars from different feedstocks for enhanced removal of heavy metals from water. *Environ Sci Pollut Res* **22**, 16640–16651 (2015).
103. *Innovation. research. sustainability. Hydrothermal carbonization of biomass and sewage sludge.*
104. The Ingelia patented HTC plant. (Castellano) Ingelia Technologies.
105. *About Our Solutions Company.* SoMax Circular Solutions. Retrieved July 23, 2023, from <https://somalxhtc.com/about-us/>
106. *Terranova Energy - together we pioneer sustainability.* TerraNova Energy GmbH. (2022, April 5)
107. Schönherr, J., Buchheim, J. R., Scholz, P., & Adelhelm, P. (2018). Boehm Titration Revisited (Part II): A Comparison of Boehm Titration with Other Analytical Techniques on the Quantification of Oxygen-Containing Surface Groups for a Variety of Carbon Materials. In *C* (Vol. 4, Issue 2, p. 22).
108. Semerciöz, A. S., Göğüş, F., Çelekli, A., & Bozkurt, H. (2017). Development of carbonaceous material from grapefruit peel with microwave implemented-low temperature hydrothermal carbonization technique for the adsorption of Cu (II). In *Journal of Cleaner Production* (Vol. 165, pp. 599–610).

109. Tasca, A.L., Puccini, M., Stefanelli, E. *et al.* Investigating the activation of hydrochar from sewage sludge for the removal of terbuthylazine from aqueous solutions. *J Mater Cycles Waste Manag* **22**, 1539–1551 (2020).
110. Ipiales, R.P., Sarrion, A., Diaz, E. *et al.* Strategies to improve swine manure hydrochar: HCl-assisted hydrothermal carbonization versus hydrochar washing. *Biomass Conv. Bioref.* (2023).
111. McCarty, K. F., Monti, M., Nie, S., Siegel, D. A., Starodub, E., El Gabaly, F., McDaniel, A. H., Shavorskiy, A., Tyliczszak, T., Bluhm, H., Bartelt, N. C., & de la Figuera, J. (2014). Oxidation of Magnetite(100) to Hematite Observed by in Situ Spectroscopy and Microscopy. In *The Journal of Physical Chemistry C* (Vol. 118, Issue 34, pp. 19768–19777).
112. Luo, X., Huang, Z., Lin, J., Li, X., Qiu, J., Liu, J., & Mao, X. (2020). Hydrothermal carbonization of sewage sludge and in-situ preparation of hydrochar/MgAl-layered double hydroxides composites for adsorption of Pb(II). In *Journal of Cleaner Production* (Vol. 258, p. 120991).
113. Xiao, Y., Ding, L., Yang, Y., Areprasert, C., Gao, Y., Chen, X., & Wang, F. (2022). Iron valence state evolution and hydrochar properties under hydrothermal carbonization of dyeing sludge. In *Waste Management* (Vol. 152, pp. 94–101).
114. Shi, Y.; Zhang, T.; Ren, H.; Kruse, A.; Cui, R. Polyethylene imine modified hydrochar adsorption for chromium (VI) and nickel (II) removal from aqueous solution. *Bioresour. Technol.* **2018**, *247*, 370–379.
115. Song, X. D., Xue, X. Y., Chen, D. Z., He, P. J., & Dai, X. H. (2014). Application of biochar from sewage sludge to plant cultivation: Influence of pyrolysis temperature and biochar-to-soil ratio on yield and heavy metal accumulation. In *Chemosphere* (Vol. 109, pp. 213–220).
116. Mihajlović, M., Petrović, J., Kragović, M., Stojanović, M., Milojković, J., Lopčić, Z., & Koprivica, M. (2017). EFFECT OF KOH ACTIVATION ON HYDROCHARS SURFACE: FT-IR ANALYSIS. In *RAD Association Journal* (Vol. 2, Issue 1). RAD Centre.
117. Niinipuu, M., Latham, K.G., Boily, JF. *et al.* The impact of hydrothermal carbonization on the surface functionalities of wet waste materials for water treatment applications. *Environ Sci Pollut Res* **27**, 24369–24379 (2020).
118. ZHANG, J., LIN, Q., & ZHAO, X. (2014). The Hydrochar Characters of Municipal Sewage Sludge Under Different Hydrothermal Temperatures and Durations. In *Journal of Integrative Agriculture* (Vol. 13, Issue 3, pp. 471–482).
119. Martins, V.M.S., Sante, L.G.G., Giona, R.M. *et al.* An inter-loop approach for hydrothermal carbonization of sewage sludge to produce hydrochars and their use as an adsorbent for iron removal from spent sulfuric acid. *Clean Techn Environ Policy* **24**, 1639–1652 (2022).

120. Oickle, A. M., Goertzen, S. L., Hopper, K. R., Abdalla, Y. O., & Andreas, H. A. (2010). Standardization of the Boehm titration: Part II. Method of agitation, effect of filtering and dilute titrant. In *Carbon* (Vol. 48, Issue 12, pp. 3313–3322).
121. He, C., Giannis, A., & Wang, J.-Y. (2013). Conversion of sewage sludge to clean solid fuel using hydrothermal carbonization: Hydrochar fuel characteristics and combustion behavior. In *Applied Energy* (Vol. 111, pp. 257–266).
122. Zhang, X., Zhang, L., & Li, A. (2017). Hydrothermal co-carbonization of sewage sludge and pinewood sawdust for nutrient-rich hydrochar production: Synergistic effects and products characterization. In *Journal of Environmental Management* (Vol. 201, pp. 52–62).
123. He, C., Zhang, Z., Ge, C., Liu, W., Tang, Y., Zhuang, X., & Qiu, R. (2019). Synergistic effect of hydrothermal co-carbonization of sewage sludge with fruit and agricultural wastes on hydrochar fuel quality and combustion behavior. In *Waste Management* (Vol. 100, pp. 171–181).
124. Brown, A. (2020). *Development and utilization of a Raman characterization method for Hydrothermal char.* : Worcester Polytechnic Institute.
125. Fidel, R. B., Laird, D. A., & Thompson, M. L. (2013). Evaluation of Modified Boehm Titration Methods for Use with Biochars. In *Journal of Environmental Quality* (Vol. 42, Issue 6, pp. 1771–1778).
126. Wu, H., Lu, W., Chen, Y., Zhang, P., & Cheng, X. (2020). Application of Boehm Titration for the Quantitative Measurement of Soot Oxygen Functional Groups. In *Energy & Fuels* (Vol. 34, Issue 6, pp. 7363–7372).
127. Deng, J., Li, X., Wei, X., Liu, Y., Liang, J., Tang, N., Song, B., Chen, X., & Cheng, X. (2019). Sulfamic acid modified hydrochar derived from sawdust for removal of benzotriazole and Cu(II) from aqueous solution: Adsorption behavior and mechanism.
128. Li, B., Lv, J.-Q., Guo, J.-Z., Fu, S.-Y., Guo, M., & Yang, P. (2019). The polyaminocarboxylated modified hydrochar for efficient capturing methylene blue and Cu(II) from water. In *Bioresource Technology* (Vol. 275, pp. 360–367).
129. He, X., Zhang, T., Xue, Q., Zhou, Y., Wang, H., Bolan, N. S., Jiang, R., & Tsang, D. C. W. (2021). Enhanced adsorption of Cu(II) and Zn(II) from aqueous solution by polyethyleneimine modified straw hydrochar. In *Science of The Total Environment* (Vol. 778, p. 146116).
130. Kalam, S., Abu-Khamsin, S. A., Kamal, M. S., & Patil, S. (2021). Surfactant Adsorption Isotherms: A Review. In *ACS Omega* (Vol. 6, Issue 48, pp. 32342–32348).
131. Kumar, A. (2023, May 28). *AIC & BIC for Selecting Regression Models: Formula, Examples*. Data Analytics.
132. Belhachemi, M., Addoun, F. Comparative adsorption isotherms and modeling of methylene blue onto activated carbons. *Appl Water Sci* **1**, 111–117 (2011).

133. Chiron, N., Guilet, R., & Deydier, E. (2003). Adsorption of Cu(II) and Pb(II) onto a grafted silica: isotherms and kinetic models. In *Water Research* (Vol. 37, Issue 13, pp. 3079–3086).
134. Huang, Y.-H., Hsueh, C.-L., Cheng, H.-P., Su, L.-C., & Chen, C.-Y. (2007). Thermodynamics and kinetics of adsorption of Cu(II) onto waste iron oxide. In *Journal of Hazardous Materials* (Vol. 144, Issues 1–2, pp. 406–411).
135. Khan, J., Lin, S., Nizeyimana, J. C., Wu, Y., Wang, Q., & Liu, X. (2021). Removal of copper ions from wastewater via adsorption on modified hematite ( $\alpha$ -Fe<sub>2</sub>O<sub>3</sub>) iron oxide coated sand. In *Journal of Cleaner Production* (Vol. 319, p. 128687).
136. Martins, V.M.S., Sante, L.G.G., Giona, R.M. *et al.* An inter-loop approach for hydrothermal carbonization of sewage sludge to produce hydrochars and their use as an adsorbent for iron removal from spent sulfuric acid. *Clean Techn Environ Policy* **24**, 1639–1652 (2022).
137. Niinipuu, M., Latham, K.G., Boily, JF. *et al.* The impact of hydrothermal carbonization on the surface functionalities of wet waste materials for water treatment applications. *Environ Sci Pollut Res* **27**, 24369–24379 (2020).
138. Lu, Y., & Miller, J. D. (2002). Carboxyl Stretching Vibrations of Spontaneously Adsorbed and LB-Transferred Calcium Carboxylates as Determined by FTIR Internal Reflection Spectroscopy. In *Journal of Colloid and Interface Science* (Vol. 256, Issue 1, pp. 41–52).
139. Ibrahim, M., Nada, A., & Kamal, D. E. (2005). Density functional theory and FTIR spectroscopic study of carboxyl group. *Indian Journal of Pure & Applied Physics*, **43**, 911–917.

# Appendix

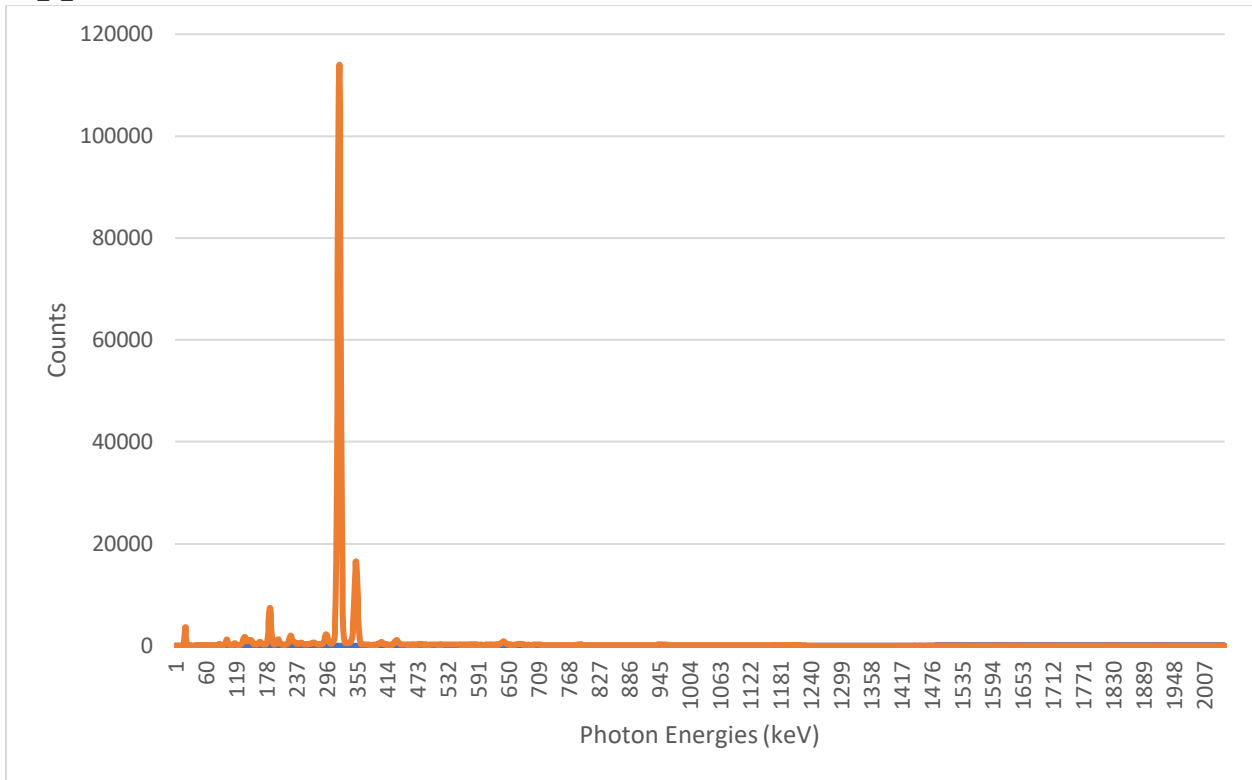


*Figure 19: XRF Spectra Unmodified SoMax Sewage Sludge*

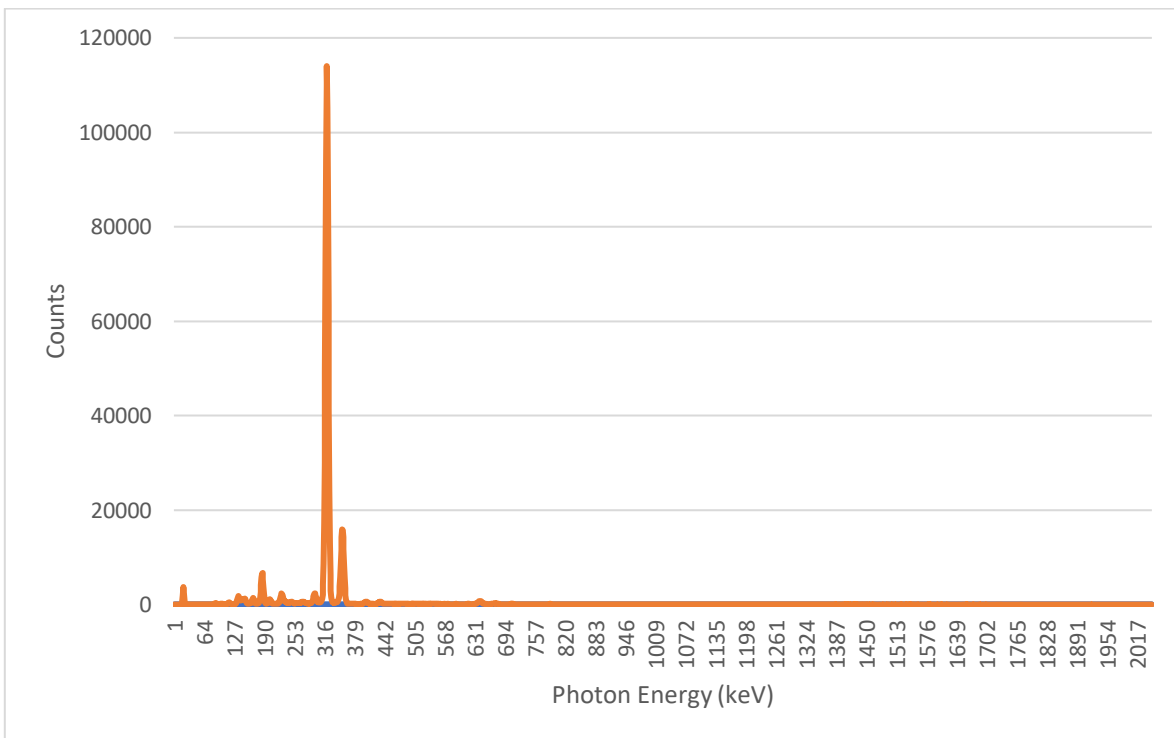


*Figure 20: XRF Spectra KOH Activated SoMax Sewage Sludge*

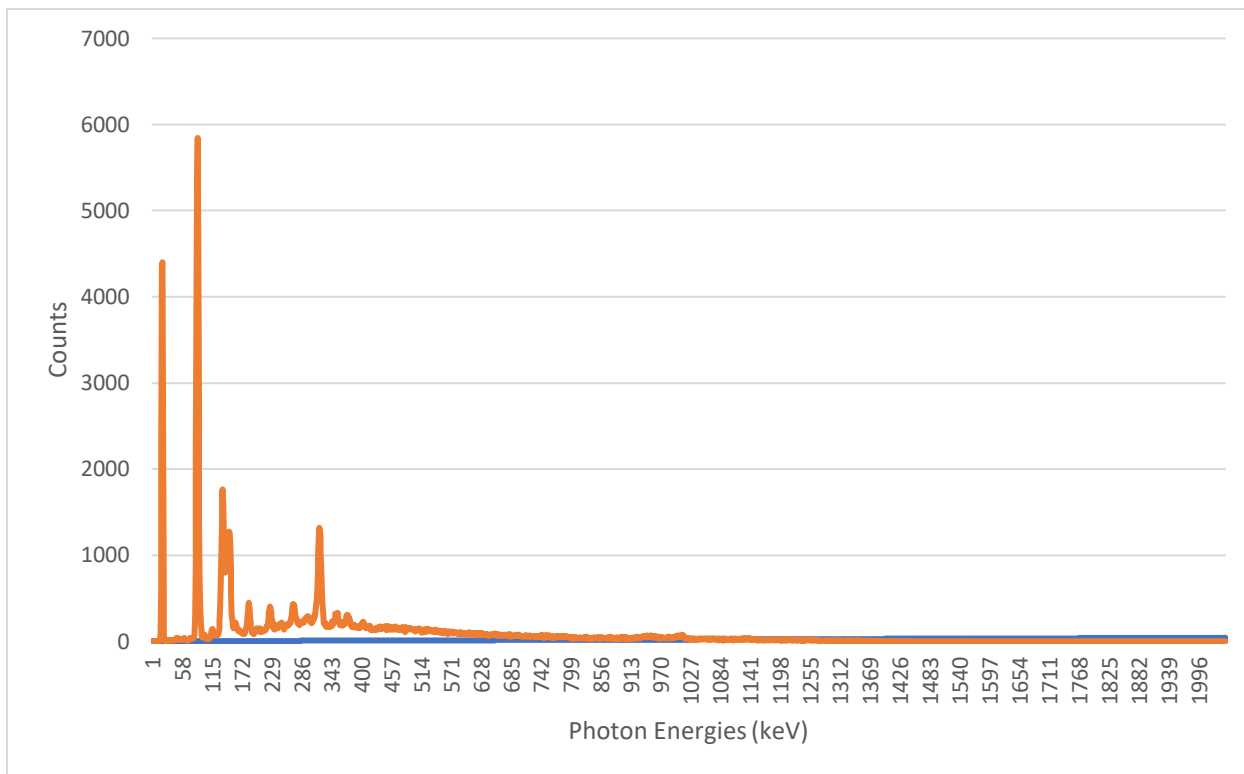


*Figure 21: XRF Spectra Silica Standard*

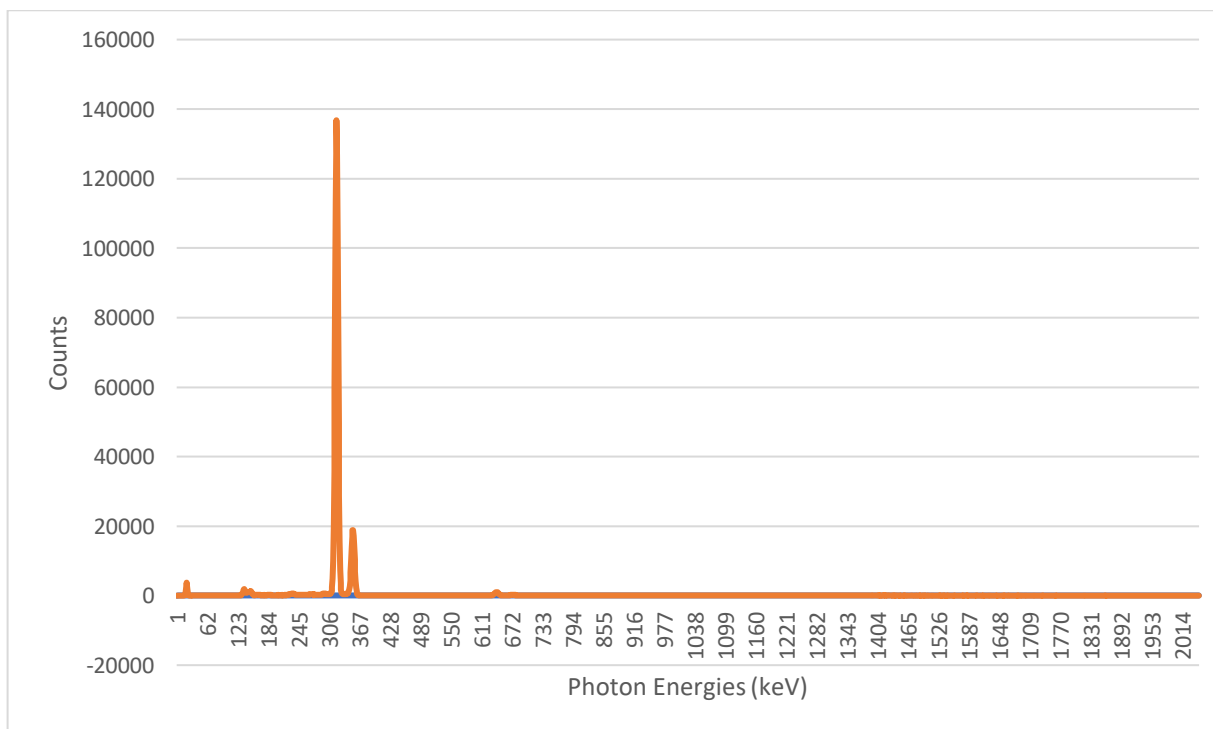


*Figure 21: XRF Spectra Iron Oxide ( $Fe_2O_3$ ) Standard*